The Structure of TGB_A and TGB_C Phases near the Lower Critical Twist

by

Venkatramanan P.R.

Thesis submitted to the Jawaharlal Nehru University for the degree of Doctor of Philosophy

2012

Raman Research Institute

Bangalore - 560080

DECLARATION

I hereby declare that this thesis is composed independently by me at the Raman Research Institute, Bangalore, under the supervision of Prof. Yashodhan Hatwalne. The subject matter presented in this thesis has not previously formed the basis of the award of any degree, diploma, associateship, fellowship or any other similar title in any other University.

(Prof. Yashodhan Hatwalne) Venkatramanan P.R.

Raman Research Institute

Bangalore

CERTIFICATE

This is to certify that the thesis entitled **The Structure of TGB_A and TGB_C Phases near the Lower Critical Twist** submitted by Venkatramanan P.R. for the award of the degree of DOCTOR OF PHILOSOPHY of Jawaharlal Nehru University is his original work. This has not been published or submitted to any other University for any other degree or diploma.

Prof. Yashodhan Hatwalne

(Centre Chairperson)

Director

Raman Research Institute

(Thesis Supervisor)

Raman Research Institute

Acknowledgements

I would like to thank my supervisor Prof. Yashodhan Hatwalne for being with me during the last six years. This work would not have been possible without his constant encouragement. I have learned a lot about how to do research, while working with him.

The work on the modulated phase in SmC was done in collaboration with Prof. N.V. Madhusudana. It has been a pleasure working with him. I thank him for his insightful comments and advice.

Many thanks Prof. Tom C. Lubensky for his inputs regarding the work on the TGB phases.

I thank the faculty, postdocs and students at RRI, with whom I have had many an interesting discussion. Without them, my stay at RRI would not have been as delightful.

My sincere thanks to the library staff, the staff at the computer centre and the RRI administration, for their support.

I am grateful to my wife Suchana, and our family, for their patience and support.

Contents

List of Figures

List of Tables

Preface

Smectics are layered systems with liquid crystalline order. The analogy of smectics with superconductors, first established by de Gennes, has proved to be immensely useful. One of the most striking consequences of this analogy has been the prediction and subsequent observation of the twist grain boundary (TGB) phases in smectic liquid crystals, which are analogues of the Abrikosov vortex phase in superconductors. Here, we study the structure of the TGB_A and the TGB_C phases, and also predict a new modulated phase in smectic-C liquid crystals.

Chapter 1 introduces continuum linear elasticity theories of liquid crystals, and discusses the smectic-superconductor analogy and its consequences. We discuss previous theoretical studies and review experimental results on TGB_A and TGB_C phases.

In Chapter 2, we show that dislocation arrays with certain geometries do not form grain boundaries in smectics. In an earlier work by Bluestein *et al.*, construction of the dislocation complexion of the TGB_A phase involves dislocation arrays which do not form grain boundaries. We propose a consistent construction for the dislocation complexion of the TGB_A phase and calculate the structural parameters of the TGB_A phase within linear theory.

In Chapter 3, we show that the covariant elasticity of SmC admits a transition into a novel modulated phase. Working with the single-wavevector ansatz, we calculate the wave-vector that minimizes the free energy in the modulated phase and find that it lies in the plane containing the layer normal and the director. We discuss an earlier experimental observation which shows a periodic stripe pattern consistent with this structure. We also discuss other thermotropic and lyotropic smectics known to exhibit modulated structures, and examine how the modulated phase we predict is different from these.

In Chapter 4, we study the energetics and interaction of dislocation lines in Smectic-C materials. We find that the lowest energy dislocation line in SmC is a mixed dislocation line. The interaction between dislocation lines in SmC turns out to be very anisotropic, and attractive (for distances much larger than the twist penetration depth) along the direction orthogonal to the c-vector. We calculate the lower critical chiral field h_{c1} for the formation of the TGB_C phase.

Modelling low angle grain boundaries as arrays of dislocation lines, we find that a grain boundary made of the minimum energy (mixed) dislocation line is energetically favourable over one that is made of screw dislocation lines. We minimize the Gibbs free energy for a rectangular TGB_C "reference lattice", and find that a lattice made of screw dislocation lines (Renn-Lubensky structure) forms the lowest energy structure. Further work on the detailed evaluation of the structural parameters of the TGB_C phase using arbitrary oblique lattices, is in progress.

Chapter 1

Introduction

1.1 Liquid crystals

Liquid crystals are a class of materials that exhibit order between that of a liquid phase and a solid phase. The molecules which make up liquid crystals are often highly anisotropic. Since their discovery by Reinitzer and Lehman in the late nineteenth century, a large number of mesogenic compounds which exhibit liquid crystalline phases with varied symmetries have been synthesized.

1.1.1 Nematics

The nematic phase typically is formed by anisotropic rod-like or disc-like molecules. At a higher temperature, the system exhibits the symmetry of liquids (symmetry under continuous translations and rotations). This phase is called the isotropic phase. Upon cooling, the system breaks rotational symmetry and forms the nematic phase. The nematic phase is characterized by the presence of orientational order (see Fig. 1.1): the positions of the molecular centres of mass remain uniformly distributed as in the liquid phase, but the direction of the long axes of the molecules has a nonzero average (given by the apolar unit vector $\mathbf{n}$ ($\mathbf{n} \equiv -\mathbf{n}$), called the *director*). The system has $\mathbf{C}_\infty$ symmetry about $\mathbf{n}$.

The broken symmetry elastic variable for the nematic phase is $\mathbf{n}$, and therefore, local changes of $\mathbf{n}$ from its equilibrium value cost energy. For small distortions, the elastic free energy for the nematic phase was first given by F. C. Frank [9] in 1958. The Frank free energy is

$$F_n = \frac{1}{2}\int \mathrm{d}^3x \,\{K_1(\nabla\cdot\mathbf{n})^2 + K_2\,[\mathbf{n}\cdot(\nabla\times\mathbf{n})]^2 + K_3\,[\mathbf{n}\times(\nabla\times\mathbf{n})]^2\}. \tag{1.1}$$

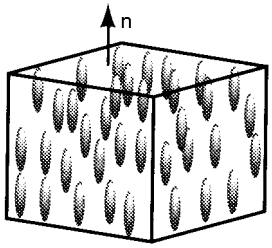

Figure 1.1: Orientation of the molecules in the nematic phase. The average direction of alignment of molecules is denoted by $\mathbf{n}$ (adopted and modified from [1]).

The K_1- term is the *splay* term, the K_2- term is the *twist* term and the K_3- term is the *bend* term. Since $\mathbf{n}$ is dimensionless, the dimensions of the Frank elastic constants K_1, K_2 and K_3 are $[\mathrm{E/L}]$ and their value is typically of the order of 10^{-7} dynes [10].

1.1.2 Cholesterics

The cholesteric phase is formed if the molecules making up the liquid crystal are intrinsically chiral, or if chiral mesogenic molecules are added to a nematic liquid crystal. The director $\mathbf{n}$ then rotates in a helical fashion (see Fig. 1.2). The pitch of the helix is typically of the order of a thousand angstroms.

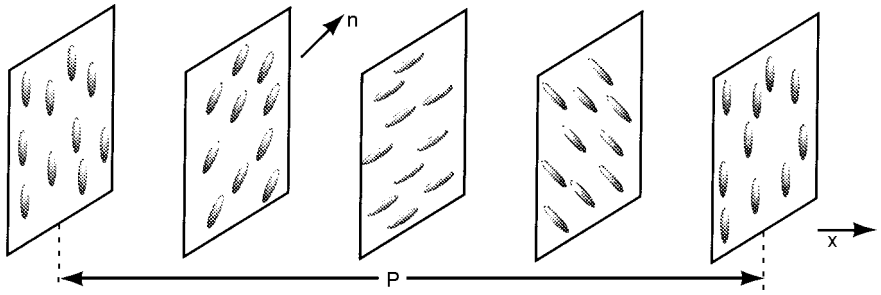

Figure 1.2: Orientation of the director in the cholesteric phase. P is the pitch of the helix, over which the director rotates by π (since $\mathbf{n} \equiv -\mathbf{n}$) (adopted and modified from [1]).

The elastic free energy in the cholesteric phase is [1]

$$F_{ch} = F_n - h \int \mathrm{d}^3x \; \mathbf{n} \cdot (\nabla \times \mathbf{n}). \tag{1.2}$$

This energy is minimized when $\mathbf{n}$ is given by

$$\mathbf{n}(\mathbf{x}) = (0, \sin\, k_0 x, \cos\, k_0 x), \tag{1.3}$$

where $k_0 = h/K_2$ because $\mathbf{n} \cdot (\nabla \times \mathbf{n}) = k_0$. We have taken the pitch axis to be along the $x-$ axis. The pseudo-scalar coefficient h is allowed in the free energy, since the cholesteric liquid crystal is chiral.

1.1.3 Smectics-A

If a nematic liquid crystal is cooled further, it may undergo a phase transition to the smectic phase. The Smectic-A (SmA) phase is made up of fluid layers of the molecules, stacked one on top of the other. In SmA, the director $\mathbf{n}$ and the layer normal $\mathbf{N}$ are parallel. This structure is periodic in the direction normal to the layers (see Fig. 1.3), *i.e.*, in the SmA phase, translational symmetry is broken along the direction given by $\mathbf{N}$. The broken symmetry elastic variable in the SmA phase is the field $u(\mathbf{x})$, which measures the local displacement (along $\mathbf{N}$) of the layers. Therefore the linear elastic free energy in this phase can be written in terms of the gradients of the u- field as [11]

$$F_A = \frac{1}{2} \int \mathrm{d}^3x \, \left[B(\nabla_\parallel u)^2 + K_1(\nabla_\perp^2 u)^2 \right] \tag{1.4}$$

where $\nabla_\parallel = \mathbf{N} \cdot \nabla$ and $\nabla_\perp = \nabla - (\mathbf{N} \cdot \nabla)\mathbf{N}$.

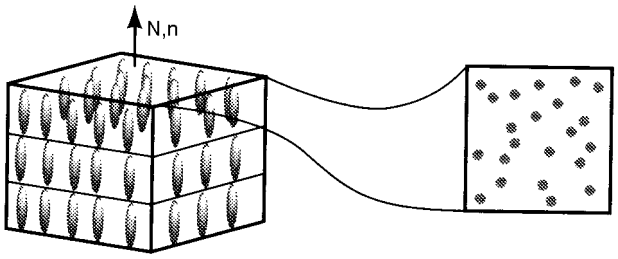

Figure 1.3: Layer structure and orientation of the molecules in the SmA phase. The average direction of alignment of molecules is denoted by $\mathbf{n}$. Layer normal is denoted by $\mathbf{N}$ (adopted and modified from [1]).

1.1.4 Smectics-C

In the Smectic-C (SmC) phase, in the absence of elastic distortions, the director $\mathbf{n}_0$ makes a constant angle A_0 with respect to the layer normal $\mathbf{N}_0$ (see Fig. 1.4). The projection of $\mathbf{n}_0$

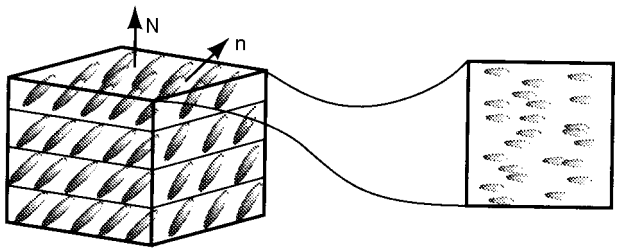

Figure 1.4: Layer structure and orientation of the molecules in the SmC phase. Layer normal is denoted by $\mathbf{N}$. The direction of average alignment of molecules, denoted by $\mathbf{n}$ is tilted with respect to the layer normal (adopted and modified from [1]).

onto the plane of the layers is the vector $\mathbf{c}_0$. The system is invariant under the simultaneous transformations $\mathbf{c}_0 \to -\mathbf{c}_0$ and $\mathbf{N}_0 \to -\mathbf{N}_0$. The $\mathbf{N}_0$-$\mathbf{c}_0$ plane is a mirror plane.

The elasticity theory for the SmC phase can be written in terms of the following fields:
1. The layer displacement field u, measuring the displacement of the smectic layers along the direction perpendicular to the smectic planes.
2. The rotation of the director tilt direction (which can also be described using the c-director) given by the (small) angles Ω_x, Ω_y and Ω_z.
We can write

$$\Omega_x = \frac{\partial u}{\partial y},\ \Omega_x = -\frac{\partial u}{\partial x}, \tag{1.5}$$

which implies that

$$\frac{\partial \Omega}{\partial x} + \frac{\partial \Omega}{\partial y} = 0. \tag{1.6}$$

Since a uniform rotation of the entire system does not cost energy, the elastic free energy must be a function of the gradients of Ω. The small rotation angle $\mathbf{\Omega} = (\Omega_x, \Omega_y, \Omega_z)$ is a psuedovector, and hence the elastic free energy will contain only terms in $(\nabla\mathbf{\Omega})^2$. In addition, a change in the layer spacing has an associated energy cost which depends on

$$\gamma = \frac{\partial u}{\partial z}. \tag{1.7}$$

There will a be term proportional to γ^2 in the free energy density which measures the changes from the equilibrium layer spacing.

We can write the elastic free energy for the smectic-C phase as

$$F_{el} = F_c + F_s + F_{cs}, \tag{1.8}$$

where

$$F_c = \frac{B_1}{2}\left(\frac{\partial \Omega_z}{\partial x}\right)^2 + \frac{B_2}{2}\left(\frac{\partial \Omega_z}{\partial y}\right)^2 + \frac{B_3}{2}\left(\frac{\partial \Omega_z}{\partial z}\right)^2 + \frac{B_{13}}{2}\left(\frac{\partial \Omega_z}{\partial x}\right)\left(\frac{\partial \Omega_z}{\partial z}\right) \tag{1.9}$$

is associated with the distortions of the **c**-director [12],

$$F_s = \frac{A}{2}\left(\frac{\partial \Omega_x}{\partial x}\right)^2 + \frac{A_{12}}{2}\left(\frac{\partial \Omega_y}{\partial x}\right)^2 + \frac{A_{21}}{2}\left(\frac{\partial \Omega_x}{\partial y}\right)^2 + \frac{\bar{B}}{2}\gamma^2, \tag{1.10}$$

in which the terms A, A_{12}, A_{21} are associated with the curvature of the smectic layers, and the $\bar{B}$ term is the layer compression term, and

$$F_{cs} = C_1\left(\frac{\partial \Omega_x}{\partial x}\right)\left(\frac{\partial \Omega_z}{\partial x}\right) + C_2\left(\frac{\partial \Omega_x}{\partial y}\right)\left(\frac{\partial \Omega_z}{\partial y}\right) \tag{1.11}$$

couples the layer distortions with the distortions in the **c**-director [13]. The coefficients A, A_{12} , A_{21}, B_1, B_2, B_3, B_{13}, C_1 and C_2 have the dimensions of energy per length. The coefficient $\bar{B}$ has the dimensions of energy per volume.

1.2 Analogy of smectics with superconductors

The analogy of the Nematic to Smectic-A transition with the normal metal to superconductor transition was first pointed out by de Gennes [14]. At the transition from the nematic phase to the smectic phase, the system breaks continuous translational symmetry along a single direction. Thus, smectics are one dimensional "solids" which are periodic along a single direction. As shown by Landau and Peierls [11], such systems cannot have true long range order, unlike solids. Also, the density correlations in the broken symmetry direction die out algebraically, rather than exponentially as for liquids [15]. The order parameter for the N-SmA transition is the complex amplitude of the first harmonic $\psi e^{i\mathbf{q}_0\cdot\mathbf{x}}$ of the complex mass density wave $\rho(\mathbf{x}) = \rho_0 + (\psi e^{i\mathbf{q}_0\cdot\mathbf{x}} + c.c) + \ldots$, where $\mathbf{q}_0 = 2\pi/d\mathbf{n}_0 = 2\pi/d\mathbf{e}_z$, and $\psi = |\psi|\, e^{-iq_0 u}$. The Ginzburg-Landau Free energy for the transition can be written as [1]

$$F = F_\psi + F_n \tag{1.12}$$

TGB phase : Liquid crystals	**Abrikosov phase : Superconductors**
Complex amplitude ψ of the mass density wave	Order parameter ψ of the superconductor-normal metal transition
Nematic director $\mathbf{n}$	Magnetic vector potential $\mathbf{A}$
Twist field $h = K_2 (\mathbf{n}_0 \cdot \nabla \times \mathbf{n}_0)$ Average twist $k_0 = V^{-1} \int \mathrm{d}^3x\, \mathbf{n} \cdot \nabla \times \mathbf{n}$	Magnetic field $\mathbf{H}$ Magnetic induction $= V^{-1} \int \mathrm{d}^3x\, \nabla \times \mathbf{A}$
Smectic A phase	Meissner phase
Nematic phase	Normal metal
Cholesteric phase	Normal metal in a magnetic field
Twist Expulsion	Meissner effect
Twist penetration depth λ_2	London penetration depth λ
Smectic correlation length ξ	Coherence length for superconducting order ξ
Twist Ginzburg parameter $\kappa = \lambda_2/\xi$	Ginzburg parameter $\kappa = \lambda/\xi$
Smectic layer spacing d	Magnetic flux quantum $\Phi_0 = h/2e$
Screw dislocation	Magnetic flux tube (vortex)
Twist grain boundary phase	Abrikosov vortex lattice phase
Chiral line liquid	Melted vortex phase

Table 1.1: Analogy between the TGB phase in smectic liquid crystals and the Abrikosov phase in superconductors (Courtesy: [2]).

where,

$$F_\psi = \int \mathrm{d}^3x \left[r\,|\psi|^2 + c_\parallel \left|\nabla_\parallel \psi\right|^2 + c_\perp \left|(\nabla_\perp + iq_0\delta\mathbf{n})\psi\right|^2 + \frac{1}{2} g\,|\psi|^4 \right] \tag{1.13}$$

and, and F_n is the Frank free energy for the director given in Eq. (1.1). The $(\nabla_\perp + iq_0\delta\mathbf{n})\psi$ term is a covariant derivative, which ensures the invariance of the Eq. (1.12) under rigid rotations of the whole system. The N-SmA transition occurs when $r = r_0(T - T_{\mathrm{NA}})$ changes sign.

The free energy Eq. (1.13) is mathematically identical to the free energy describing the normal metal - superconductor transition. This leads to a very useful analogy between the normal metal - superconductor transition and the N-SmA transition (see Table 1.1). Importantly, the deviation of the nematic director from its equilibrium value, $\delta\mathbf{n}$, is the analogue of the electromagnetic vector potential $\mathbf{A}$ in superconductors.

The analogy of smectics with superconductors can be taken further. Superconductors expel magnetic field. This is known as Meissner effect [16]. In a superconductor placed in a magnetic field, the magnetic field penetrates into the superconductor only upto a certain characteristic length, known as the London penetration depth. The Ginzburg parameter is defined as $\kappa = \lambda/\xi$, where λ is the the magnetic field penetration depth and ξ is the coherence length of the superconducting order parameter. For $\kappa < 1/\sqrt{2}$, the superconductor is labelled as type-I and

for $\kappa > 1/\sqrt{2}$, as type-II. The response of a superconductor to the presence of a magnetic field depends on its nature (type-I or type-II). In type-I superconductors, as the magnetic field is increased, beyond a critical value of the magnetic field h_c, the superconducting order breaks down and the system becomes a normal metal. In type-II superconductors, as the magnetic field is increased beyond a critical value h_{c1}, the the magnetic field penetrates the superconducting medium as flux tubes. These flux tubes arrange as a two dimensional triangular lattice, and give rise to the Abrikosov vortex lattice phase. As the magnetic field is increased further, beyond a value h_{c2}, superconducting order completely breaks down and the system turns into a normal metal. The phase diagram is shown in Fig. 1.5.

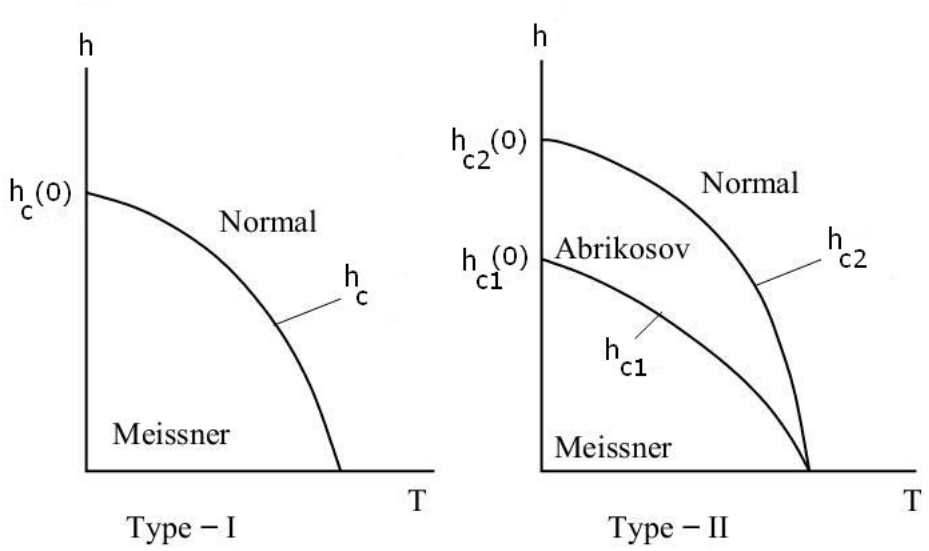

Figure 1.5: Phase diagram in the h-T plane for type-I and type-II superconductors. h is the magnitude of the magnetic field and T is the temperature. For type-II superconductors, there is an intervening Abrikosov vortex lattice phase in between the superconductor and normal metal phases (Courtesy: [2]).

de Gennes [14] noted that like in superconductors, there are two important length scales in smectics: (*i*) The smectic correlation length ξ, which is the analogue of the coherence length in superconductors, and, (*ii*) The penetration depth λ, which is the analogue of the London penetration depth in superconductors. The Ginzburg parameter κ for smectics is given in terms of these characteristic lengths, by $\kappa = \lambda/\xi$. In analogy with superconductors, we can then define type-I ($\kappa \leq 1/\sqrt{2}$) and type-II ($\kappa > 1/\sqrt{2}$) smectics. This allows for the possibility of there being an analogue of the Abrikosov vortex phase in smectics. de Gennes suggested a

structure made of a lattice of edge dislocations. Although it was de Gennes who first realized this possibility, the exact structure of the of this phase was first predicted by Renn and Lubensky [17]. They argued that the proper analogue of the magnetic field in the case of smectics is the twist $\mathbf{n} \cdot (\nabla \times \mathbf{n})$, and that the analogue of the London penetration depth is the twist penetration depth $\lambda_2 = K_2/D$, where K_2 is the modulus of twist deformations of the director, as defined in Eq. (1.1), and D is the coefficient of the covariant term in Eq. (1.13). In this picture, the analogue of a flux tube is a screw dislocation line, and that of the Abrikosov vortex phase is the twist grain boundary phase in smectics.

A low temperature elasticity theory ($r < 0$) of Smectics can be developed by taking the amplitude of the order parameter to be a constant and considering only the fluctuations in its phase. The deviations of the phase from its equilibrium value can be taken into account by introducing the layer displacement field $u(\mathbf{x})$, defined through the equation $\psi = |\psi|\, e^{i(\mathbf{q}_0 \cdot \mathbf{x} - q_0 u(\mathbf{x}))}$. When u- is independent of x, it defines the set of uniformly spaced smectic layers. Deviations from the uniform smectic ground state are characterized by a spatially varying $u(\mathbf{x})$. Thus, in the smectic phase, $u(\mathbf{x})$ is the broken symmetry elastic variable. In this limit, the Eq. (1.12) reduces to [1]

$$\begin{aligned} F_{\rm el} = & \frac{1}{2} \int \mathrm{d}^3x \left[B(\nabla_\parallel u)^2 + D(\nabla_\perp u + \delta n)^2 \right] \\ & + \frac{1}{2} \int \mathrm{d}^3x \left[K_1 (\nabla \cdot \mathbf{n})^2 + K_2 \left(\mathbf{n} \cdot (\nabla \times \mathbf{n})\right)^2 + K_3 \left(\mathbf{n} \times (\nabla \times \mathbf{n})\right)^2 \right] \end{aligned} \tag{1.14}$$

where $B = c_\parallel q_0^2 \left|\psi\right|^2$ and $D = c_\perp q_0^2 \left|\psi\right|^2$.

1.3 Covariant Elasticity of Smectic-C

Hatwalne and Lubensky [18] gave a unified description of the covariant elasticity of both SmA and SmC liquid crystals. To understand their procedure, it is useful to parametrize the quantities of interest the following manner. In SmA liquid crystals, the Frank director $\mathbf{n}_0$ is spatially uniform and parallel to the layer normal $\mathbf{N}_0$ ($\mathbf{n}_0 \cdot \mathbf{N}_0 = 1$), whereas in SmC, $\mathbf{n}_0$ is tilted at an angle to $\mathbf{N}_0$, *i.e.*, $\mathbf{n}_0 \cdot \mathbf{N}_0 = \cos A_0 = \alpha$, where A_0 is the equilibrium tilt angle between the Frank director and the layer normal. The equilibrium **c**-vector $\mathbf{c}_0$ is defined as the projection of $\mathbf{n}_0$ onto the plane of the layers. Therefore, $\mathbf{c}_0 \cdot \mathbf{N}_0 = 0$. We will take $\mathbf{N}_0$ to be along the $z-$ axis. The layer normal can be written in terms of ∇u as

$$\mathbf{N} \simeq (-\nabla_\perp u, 1) \tag{1.15}$$

In the SmA phase, the distortions of $\mathbf{n}_0$ from its equilibrium value can be characterized by $\delta\mathbf{n}$ (to the linear order in deviations $\delta\mathbf{n}$) as

$$\mathbf{n} \simeq (\delta\mathbf{n}, 1), \tag{1.16}$$

and in the SmC phase, we can write

$$\mathbf{n} = (\mathbf{c}, \sqrt{1 - c^2}), \tag{1.17}$$

where

$$\mathbf{c} = (c_0 + \delta c)(\sin\phi, \cos\phi, 0). \tag{1.18}$$

The linear deviations of $\mathbf{c}$ from its equilibrium value $\mathbf{c}_0 = c_0(1, 0, 0)$ is given by

$$\delta\mathbf{c} = (\delta c, c_0\delta\phi, 0), \tag{1.19}$$

and thus,

$$\delta\mathbf{n} = (\delta c, c_0\delta\phi, -\frac{c_0\delta c}{\cos A_0}). \tag{1.20}$$

Starting from the premise that the elastic free energy in both the SmA and the SmC phase can depend only on change in the relative angle, $\delta(\mathbf{n}\cdot\mathbf{N})$, between $\mathbf{n}$ and $\mathbf{N}$, the inverse layer spacing q_s in the smectic phase, and the rotationally invariant gradients of u, [18] derive the elastic free energy density in the SmA phase as

$$f_A = \frac{1}{2}B\,(\nabla_z u)^2 + \frac{1}{2}D\,(\delta\mathbf{n} + \nabla_\perp u)^2 + \frac{1}{2}K_u\,(\nabla_\perp^2 u)^2 + f_n \tag{1.21}$$

where f_n is the Frank free energy density for nematics (see Eq. (1.1)), and the elastic free energy density in the SmC phase as

$$\begin{aligned} f = (1/2)[&B\,(\partial_z u)^2 + D\,(\delta c + \alpha\,\partial_x u)^2 \\ &- 2L\,(\delta c + \alpha\,\partial_x u)(\partial_z u) + K_u\,(\nabla^2 u)^2 \\ &+ K_c\,(\nabla\delta c)^2 + K_\phi\,(\nabla\delta\phi)^2], \end{aligned} \tag{1.22}$$

The terms with coefficients B and K_u are familiar from the Landau-Peierls elastic free energy for SmA [11]. These account for layer-compression and layer-bend energies respectively. The Frank free energy for distortions in the director field is represented via terms with coefficients K_c and K_ϕ in the one-constant approximation [10]. The $D-$ and L terms involve the covariant form

$(\delta c + \alpha\, \partial_x u)$ which measures the deviation $\delta(\mathbf{n}\cdot\mathbf{N})$ from its equilibrium value α. The term with the coefficient L is allowed by the symmetry of SmC, and couples the covariant form to changes in the equilibrium layer spacing. The elastic constants B, D, K_u, K_c and K_ϕ have to be positive for stability. Stability conditions do not restrict the sign of L. Notice that the term involving $\delta\phi$-field is not coupled to the u- and δc- fields.

1.4 Scale dependence of elastic constants

Calculations by de Gennes [19] and Jahnig and Brochard [20] have predicted that the Frank elastic constants K_1 and K_2 diverge as the correlation length ξ, as one approaches the Nematic-SmA transition temperature T_{NA}, whereas K_1 remains well behaved. For the Nematic-SmC transition, they have predicted that all the three Frank elastic constants diverge near T_{NC}. In the calculation by de-Gennes, these diverge as $\xi^{\frac{3}{2}}$.

Chen and Lubensky [21] proposed a Ginzburg-Landau theory to describe both N-SmA and N-SmC transitions, with the phase boundaries meeting at a Lifshitz point. The order parameter they work with is $m(\mathbf{r}) = \int_D \frac{\mathrm{d}^3k}{(2\pi)^3} e^{\mathbf{i}\mathbf{k}\cdot\mathbf{r}}\rho(\mathbf{k})$, where $\rho(\mathbf{k})$ is the Fourier transform of the density $\rho(\mathbf{r})$, and D is a two-part domain (excluding $\mathbf{k}=0$), centred around $(q_{||}, 0, 0)$ and containing the circles $k_{||} = \pm q_{||}, |k_\perp| = |q_\perp|$. They work with a Ginzburg-Landau Hamiltonian H which can be written as sum of three parts:

$$\beta H = \beta H_m + \beta H_{el} + \beta H_4 \tag{1.23}$$

where βH_{el} is the elastic Frank free energy of nematics given in Eq. (1.1), and βH_m and βH_4 are given as

$$\beta H_m = \frac{1}{2}\int \mathrm{d}^3r\, \beta h_m, \tag{1.24}$$

with

$$\begin{aligned}\beta h_m = \big(a\, m^2 + D_{||}\,[(\mathbf{n}\cdot\nabla)^2 m]^2 - C_{||}\,[\mathbf{n}\cdot\nabla m]^2 + (C_{||}^2/4D_{||})\, m^2 \\ + C_\perp\, \delta_{ij}^T\, \nabla_i m \nabla_j m + D_\perp\, (\nabla_\perp^2 m)^2\big)\,,\end{aligned} \tag{1.25}$$

and,

$$\beta H_4 = u\int \mathrm{d}^3r\, m^4(\mathbf{r}) \tag{1.26}$$

where $\mathbf{n}$ is the Frank director. $\delta_{ij}^T = \delta_{ij} - n_i n_j$ is the projection operator onto the plane perpen-

dicular to $\mathbf{n}$, $\nabla_\perp^2 = \delta_{ij}^T \nabla_i \nabla_j$ and $a = a'(T - T_{NA})$ changes sign at the Nematic-SmA transition

Their calculation predicts the critical exponents for both the N-SmA transition and N-SmC transition. A perturbative renormalization group calculation is done to show that the Frank elastic constants K_2 and K_3 diverge as T_{NA} is approached, whereas K_1 is well-behaved. As T_{NC} is approached, and all three Frank elastic constants diverge as ξ^2.

Grinstein and Pelcovitz [22] have performed a renormalization group calculation including anharmonic terms. They have shown that the layer compression modulus B vanishes and that the modulus of layer bend K_u diverges logarithmically, with system size. However, the length scale over which these effects become relevant is very large. They are not of any relevance at laboratory lengthscales.

1.5 Dislocations

Deformations of an elastic medium can be described by a displacement field $\mathbf{u}(\mathbf{x})$ that measures the displacement of each point in the medium from its original undistorted position. In an elastic medium, strains can be produced not by external forces alone, but also by the presence of internal defects, such as dislocations, in the periodic structure of the medium.

1.5.1 Dislocation lines in crystals

The elastic variable in a periodic crystal is the vector displacement field $\mathbf{u}(\mathbf{x})$. A dislocation line in a crystal is defined by [1]

$$\oint \mathrm{d}\mathbf{u} = \oint \frac{\mathrm{d}\mathbf{u}}{\mathrm{d}s}\mathrm{d}s = \mathbf{R} = \mathbf{b}, \tag{1.27}$$

where $\mathbf{R}$ is a direct lattice vector, and the Burgers vector $\mathbf{b}$ belongs to the set of direct lattice vectors. The integral is over a closed loop which encircles the dislocation line and s is the arclength. The Burgers vector and the direction of the dislocation core uniquely specify the type of the dislocation line. For an edge dislocation line, $\mathbf{b}$ is perpendicular to the core of the dislocation line, and for a screw dislocation line, $\mathbf{b}$ is along the direction of the core. Dislocation lines with both an edge and a screw component are called mixed dislocation lines. For a mixed dislocation line, the Burgers vector is at an angle to the core.

1.5.2 Dislocations in smectics

In smectics, deformation from the regular periodic structure is given by the displacement field $u(\mathbf{x})$, which measures displacement along the direction of the layer normal (chosen here to be along the z- axis). The deformed smectic planes are defined by [1]

$$z - u(\mathbf{x}) = k\,d = \frac{2\,\pi\,k}{q_0}. \tag{1.28}$$

The dislocation line in a smectic medium is defined by the relation

$$\oint \mathrm{d}\mathbf{u} = \mathbf{b} = k\,d\,\mathbf{e}_z. \tag{1.29}$$

The above equation implies that, if we sum over the displacements on a closed loop encircling the dislocation line, the layers undergo a net displacement of $k\,d$. The vector $\mathbf{b} = k\,d\,\mathbf{e}_z$ is called the Burgers vector of the dislocation line. The set of Burgers vectors is equivalent to the direct lattice specifying the equilibrium positions of the smectic planes. Since the smectic is periodic only along a single direction, the $\mathbf{b}$ always points along the layer normal.

In the core of a dislocation line, the layer displacement field is singular, which means that the u- field cannot be uniquely defined. In this region, smectic order vanishes and the medium is in a higher symmetry state, *i.e.*, a nematic.

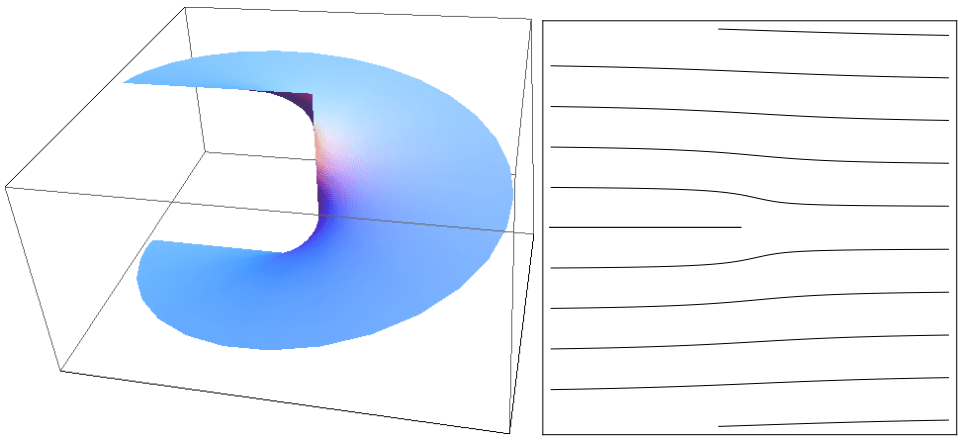

(a) Screw (b) Edge

Figure 1.6: Layer structure in the presence of a (a) screw and (b) edge dislocation line in smectics. (a) shows the displacement of the layer over one circuit of the dislocation core. (b) shows a half-layer that has been inserted, so as to form an edge dislocation line.

The nature of the dislocation line depends on the relative orientation of the dislocation core (specified by the vector $\mathbf{l}$) and the Burgers vector $\mathbf{b}$. If $\mathbf{l}$ is parallel to $\mathbf{b}$, the dislocation line is called a screw-dislocation. If $\mathbf{l}$ is perpendicular to $\mathbf{b}$, the dislocation line is called an edge-dislocation. A screw dislocation can be thought of as a being formed by a set of smectic planes which go around the defect core in a screw-like manner (see Fig. 1.6(a)). The smectic layer displacement field in this configuration is given by

$$z - \frac{d}{2\,\pi} \arctan \frac{y}{x} = k\,d. \tag{1.30}$$

For a right handed screw, $\mathbf{b}\cdot\mathbf{l} = b$ and for a left-handed screw, $\mathbf{b}\cdot\mathbf{l} = -b$. An edge dislocation can be thought of as being produced by inserting (or equivalently, removing) a half plane from the periodic one-dimensional lattice (see Fig. 1.6(b)) . If the core of the edge dislocation lies along the x- axis, the singular part of the displacement field can be written as $(d/2\,\pi)\,\arctan(z/y)$ [1]. For an edge dislocation, $\mathbf{b}\cdot\mathbf{l} = 0$. Dislocation lines for which $\mathbf{l}$ is neither parallel nor perpendicular to $\mathbf{b}$, but makes an angle γ with respect to $\mathbf{b}$, are called mixed dislocation lines.

1.6 Grain boundaries

Grain boundaries are interfaces between stress-free regions with different orientation [3], in a system with discrete translational symmetry (*e.g.,* crystals, smectic liquid crystals, quasicrystals). At large distances from the grain boundary, the lattice vectors on either side of the grain boundary are related to each other by a pure rotation.

1.6.1 Grain Boundaries in crystals

A grain boundary in a three dimensional crystal has five degrees of freedom: three corresponding to the relative orientation of the two adjacent grains, and two describing the orientation of the grain boundary with respect to these two grains. The angle by which the adjacent grains are rotated relative to each other, $\mathbf{\Omega}$, lies in the plane of the grain boundary for a tilt grain boundary (made of edge dislocation lines). For a twist grain boundary (made of screw dislocation lines), $\mathbf{\Omega}$ is perpendicular to the plane containing the grain boundary. A grain boundary can have mixed character, with both tilt and twist components. A symmetric grain boundary is one for which the surface of the boundary is oriented symmetrically with respect to the two grains.

A small-angle grain boundary ($\mathbf{\Omega}$ small) can be modelled as an array of the appropriate kind of dislocation line. A large-angle grain boundary, though, cannot be modelled as an array of

dislocations. This is because the dislocation density in the plane of the grain boundary would need to be large in order to produce the large relative rotation of the grains. At such large dislocation densities, the cores of the dislocations making the grain boundary would overlap, and the concept individual dislocation lines would become meaningless. A symmetric tilt grain boundary is the simplest in terms of structure. It can be modelled as an array of edge dislocations.

Frank's formula gives the dislocation content in a small-angle grain boundary. Consider a grain boundary composed of parallel, equally spaced dislocation lines between two adjoining grains $\mathbf{A}$ and $\mathbf{A}'$. Let $\mathbf{L}$ be a lattice vector in the plane of the boundary with indices $[\mathbf{h}, \mathbf{k}, \mathbf{l}]$ referred to the lattice $\mathbf{A}$. Let $\mathbf{L}'$ be another lattice vector with the same crystallographic indices $[\mathbf{h}, \mathbf{k}, \mathbf{l}]$, referred to the grain $\mathbf{A}'$ (see Fig. 1.7). The difference $\mathbf{b}_{tot}(\mathbf{L}) = \mathbf{L} - \mathbf{L}'$ can be expressed as an integer linear combination of the Burgers vectors $\mathbf{b}_i$:

$$\mathbf{b}_{tot}(\mathbf{L}) = \sum_i a_i(\mathbf{L})\, \mathbf{b}_i, \tag{1.31}$$

where $a_i(\mathbf{L})$ is the number of dislocations with Burgers vector $\mathbf{b}_i$ cut by $\mathbf{L}$. If the rotation angle between the grains is $\mathbf{\Omega}$, then

$$\mathbf{b}_{tot}(\mathbf{L}) = \mathbf{L} \times \mathbf{\Omega}, \tag{1.32}$$

for small angles of rotation. This equation shows that the Burgers vector content of the grain boundary increases with length, and is known as Frank's formula. For a small angle symmetric tilt grain boundary, $|\mathbf{\Omega}| = b/l_d$, where l_d is the separation between the dislocations in the grain boundary.

A twist grain boundary in a crystal is more complicated, consisting of two sets of mutually perpendicular arrays of dislocation lines [18].

1.6.2 Grain boundaries in smectics

Smectic liquid crystals are characterized by fluid order in the plane of the layers. This has consequences for the structure of grain boundaries in smectics. For instance, unlike in crystals, a twist grain boundary in smectics does not involve a mutually orthogonal pair of dislocation arrays. It is composed of a single array of screw dislocation lines. We will discuss the topology and geometry of grain boundaries in smectics in detail, in Chapter 2.

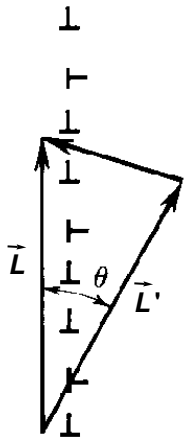

Figure 1.7: L and L' point in the same crystallographic direction (h,k,l) in the tow adjoining grains. The difference $L - L'$ is the sum of the Burgers vectors of the dislocations enclosed by the closed triangle in the figure. Dislocations are shown by $\perp$ (adopted and modified from [3]).

1.7 The TGB$_A$ Phase

Although the possibility of an analogue of the Abrikosov vortex phase in smectics was suggested by de Gennes, the exact structure of such a phase, the twist grain boundary phase, was predicted by Renn and Lubensky in 1988 [17]. However, unlike the Abrikosov vortex lattice, the structure of the TGB-A phase is not that of a two-dimensional lattice of screw-dislocations, since such a structure has an energy that diverges with system size and is not stable in the thermodynamic limit (as pointed out by Sethna [17]). Instead, the structure of the TGB phase is as shown in Fig. 1.8: slabs consisting of smectic planes, separated by grain boundaries made up of screw dislocations.

The experimental discovery of the the TGB$_A$ phase was almost concurrent with its theoretical prediction by Renn and Lubensky. Goodby and co-workers [23] observed the TGB$_A$ phase in the homologous series of the compound $\mathrm{nP1M7}$. Optical measurements showed a helical structure and x-ray diffraction confirmed the existence of smectic layering. The detailed nature of the grain boundaries was shown in a later paper [24], where they performed freeze fracture microscopy and found that the grain boundaries were formed by screw dislocations and were oriented perpendicular to the helical axis.

The ratio of the l_b (distance between the grain boundaries) to l_d (distance between individual dislocation lines in a grain boundary) (see Fig. 1.8) was calculated within linear theory by

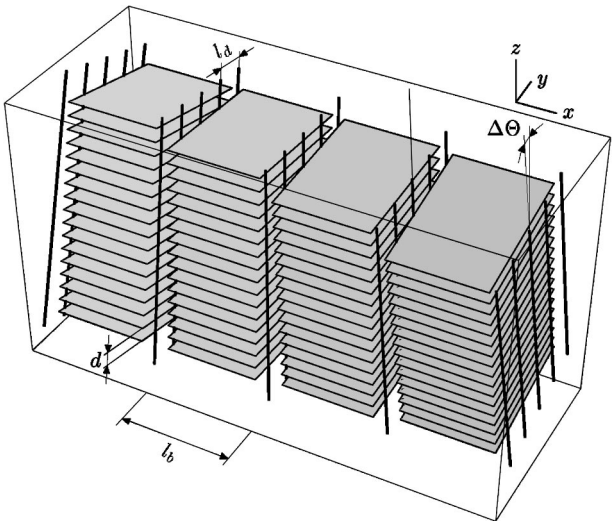

Figure 1.8: Structure of the TGB$_A$ phase. l_b is the distance between grain boundaries, and l_d is the distance between dislocation lines in a grain boundary. Adjacent smectic slabs are rotated with respect to each other by an angle $\Delta\theta$ (Courtesy: [4]).

Bluestein, Kamien and Lubensky [4]. They used the harmonic elastic free energy

$$F = \frac{1}{2}\int \mathrm{d}^3x \, \left[B\left(\nabla_z u\right)^2 + D\left(\nabla_\perp u - \delta\mathbf{n}\right)^2 + K_1\left(\nabla_\perp \cdot \delta\mathbf{n}\right)^2 + K_2\left(\nabla_\perp \times \delta\mathbf{n}\right)^2 + K_3\left(\nabla_z \delta\mathbf{n}\right)^2\right] \tag{1.33}$$

Under the assumption that the grain boundaries are made of screw dislocations, the above equation reduces to

$$F = \frac{1}{2}\int \mathrm{d}^3x \, \left[D\left(\nabla_\perp u - \delta\mathbf{n}\right)^2 + K_2\left(\nabla_\perp \times \delta\mathbf{n}\right)^2\right] \tag{1.34}$$

They take $\mathbf{v} = \nabla_\perp u$ to be the non-analytic part of the gradient of the $u-$ field, and using the fact that $\nabla \times \mathbf{v} = \mathbf{b}(\mathbf{x})$ where $\mathbf{b}(\mathbf{x}) = \mathbf{e}_z \sum_\mu k_\mu d \int ds\, \delta(\mathbf{x} - \mathbf{R}_\mu(s))$ is the dislocation density, with d being the layer spacing and k_μ the strength of the dislocation source at position $\mathbf{R}_\mu(s)$ parametrized in terms of the arclength s. They derive the Fourier space expression for the elastic free energy per unit length in the case of an arbitrary dislocation density as

$$\frac{F}{L} = \int \frac{\mathrm{d}^2q}{(2\pi)^2} \frac{1}{\mathbf{q}_\perp^2 + \lambda^{-2}} \left|\mathbf{b}(\mathbf{q}_\perp)\right|^2 \tag{1.35}$$

Working within the linear theory, [4] used the principle of superposition to calculate the energy per unit area for an array of screw dislocation lines (a low angle grain boundary). Their result closely resembles that of parallel vortices in a superconductor in the London limit. [4] also cal-

culated the interaction between two small-angle grain boundaries, which they considered to be rotated by an angle θ with respect to each other. They found that this interaction energy dies off exponential with the distance between the grain boundaries. They then proceeded to calculate the energetics of the TGB$_A$ phase, and found that within the TGB$_A$ phase, $l_b/l_d \approx 0.95$ for a wide range of values of the chiral field h.

Dozov [25] has suggested an alternative structure for grain boundaries in the TGB$_A$ phase. In this picture, called the molten grain boundary phase (MGB phase), the smectic order vanishes at the grain boundaries. This structure has not been experimentally observed.

Kamien and Lubensky have predicted a chiral line liquid phase [26], which can be thought of as a liquid of screw dislocations in the cholesteric phase. Experimental studies on this phase have been reported [27].

1.8 The TGB$_C$ Phase

The TGB$_C$ phase was predicted by Lubensky and Renn in 1990 [28]. The structure originally proposed by Lubensky and Renn had layered smectic-C slabs separated by twist grain boundaries (see Fig. 1.9). For this structure, the layer normal is perpendicular to the TGB$_C$ pitch axis and rotates around it in the successive TGB$_C$ slabs. The electric polarization vector $\mathbf{P}_S \propto \mathbf{n} \times \mathbf{N}$ lies along the TGB$_C$ pitch axis. The structure factor is qualitatively identical to that of the TGB$_A$ phase. In this section, the discussion of experimental results follows that reviewed in [29].

Nguyen *et al.* [30] and Bouchta *et al.* [31] synthesized new chiral liquid crystalline materials showing cholesteric to smectic transitions and SmA to SmC transitions in the same chiral homologous compounds $\mathrm{nF_2BTFO_1M_7}$, which exhibited the predicted TGB$_C$ phase. The structure of this phase was studied using optical microscopy and x-ray diffraction, which revealed the presence of a helical structure along with smectic layering. The detailed microscopic structure was studied by Navailles *et al.* [6] using x-ray diffraction. The structure they found is shown in Fig. 1.10. The SmC layers are tilted by an angle ω_L with respect to the helical axis. Since this angle ω_L is approximately equal to the director tilt angle, the director $\mathbf{n}$ is roughly perpendicular to the helical TGB axis, as in TGB$_A$. The electric polarization vector $\mathbf{P}_S \propto \mathbf{n} \times \mathbf{N}$ was perpendicular to the TGB$_C$ pitch axis and the ratio l_b/l_d was observed to be between 7 and 8.5.

Kundagrami and Lubensky [5] later showed that close to the upper critical twist, either the Renn-Lubensky Phase (Fig. 1.9) or the Bordeaux phase (Fig. 1.10) could become stabilized depending on a certain parameter which characterizes the system. They considered a modified

form of the Chen-Lubensky free energy $F = \int \mathrm{d}^3x\, f + F_n$, where

$$f = \Big[r|\psi|^2 + D_{||} \left|(\nabla_{\parallel}^2 + q_0^2)\psi\right|^2 + D_{\perp} \left|(\nabla_{\perp}^2 + q_0^2)\psi\right|^2 \tag{1.36}$$

$$+ D_{\parallel\perp} \left[(\nabla_{\parallel} + q_0^2)\psi^*(\nabla_{\perp}^2 + q_{0\perp}^2)\psi + c.c\right] + \frac{1}{2} g\, |\psi|^4 \Big] \tag{1.37}$$

and F_n is given in Eq. (1.1). Here, ψ is the complex mass density-wave amplitude defined through $\rho = \psi + \psi^*$. They showed that cholesteric phase becomes unstable to the Bordeaux phase when $(D_{\parallel\perp}/D_{\parallel}) < (1/\sqrt{2})$ and it becomes unstable to the Renn-Lubensky phase before the Bordeaux phase if $(D_{\parallel\perp}/D_{\parallel}) > (1/\sqrt{2})$.

For the Frank elastic constants which have $K_1, K_2 > K_3$, Renn [32] has predicted the existence of a TGB$_C^*$ phase with SmC* like ordering within the smectic slabs. Reibero *et. al.* [33] have found a TGB$_C$ phase (S-TGB$_C$) exhibiting a square grid optical pattern in planar geometry and a broad angular distribution of the layer normal relative to the TGB helix axis. Galerne [34] proposed some modifications to the Renn model of the TGB$_C^*$ phase to account for this observation.

Pullarkat *et al.* [35] have reported the discovery of a new *undulated*-TGB$_C^*$ phase, which shows a square grid pattern in the plane normal to the helix axis, and undulations of the grain boundaries with displacements along the helix axis. A model [7] to explain these observations has been suggested, which requires a helical arrangement of the molecules within the SmC^*-like blocks.

In 1993, Shao *et. al.* [36] reported some new materials which exhibited the Renn-Lubensky TGB$_C$ phase, as well as the square grid modulation at low temperatures. Fernsler *et al.* [37] have studied a compound in the same series, that exhibits a TGB$_C$ phase with very large l_b ($> 200\mathrm{nm}$). These 'giant-block' TGB (GBTGB) phases exhibit very large changes in angular orientation between adjacent slabs. Theoretical models [37] based on the fact that these are formed by extreme type-II materials account for the observed features. The grain boundaries in these materials have weak smectic ordering, and can the thought of as a melted (nematic-like) wall.

Some other models of the TGB$_C$ phase have also been proposed. Dozov [25] has proposed the melted grain boundary (MGB) phase, where the grain boundaries are are melted (nematic-like) walls, rather than being made of dislocation lines. Luk'Yanchuk has proposed a TGB$_{2q}$ phase [38] which appears as a superposition of two degenerate TGB$_C$ phases with different left and right layer inclinations.

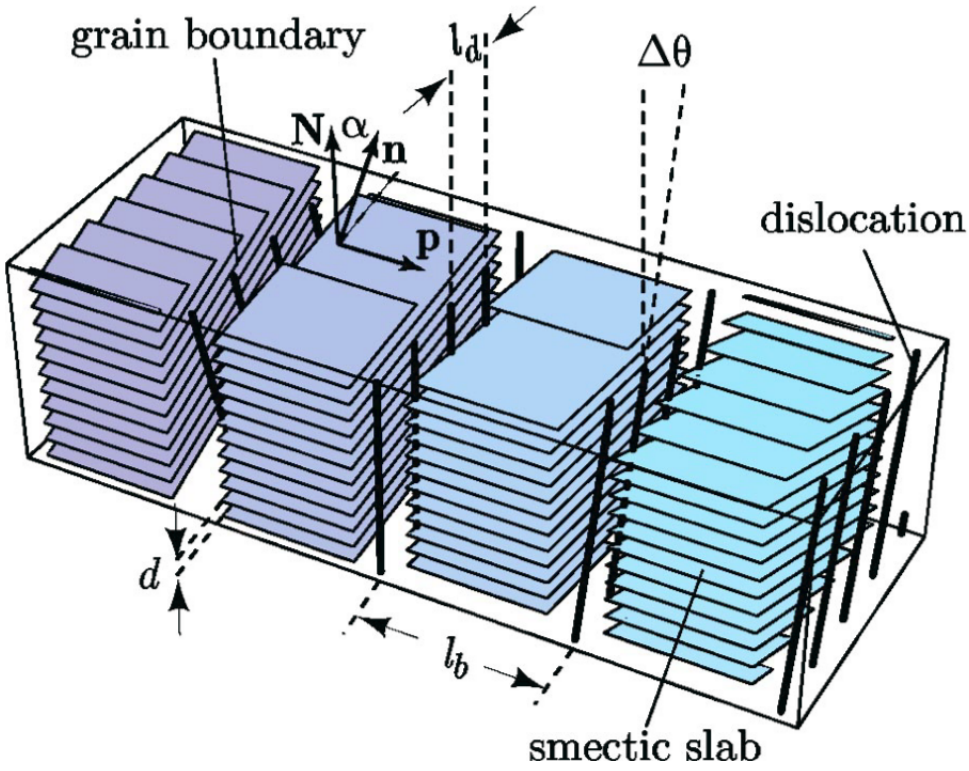

Figure 1.9: The Renn Lubensky structure of the TGB_C phase. l_b is the distance between grain boundaries, and l_d is the distance between dislocation lines in a grain boundary. α is the angle between $\mathbf{n}$ and $\mathbf{N}$, $\mathbf{p}$ is the pitch axis of the TGB_C helix and d is the spacing between the layers. $\Delta\theta$ s the angle of rotation between the adjacent smectic slabs (Courtesy: [5]).

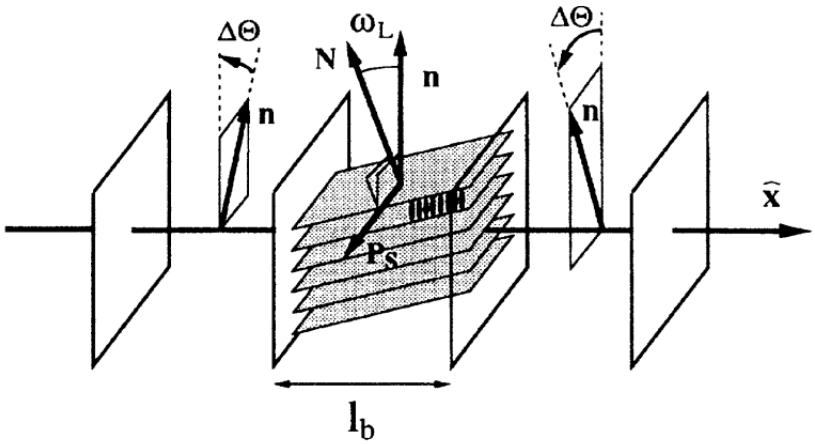

Figure 1.10: The Bordeaux structure of the TGB$_C$ phase. l_b is the distance between grain boundaries, and $\Delta\Theta$ is the angle of rotation between the successive SmC slabs. The layer normal $\mathbf{N}$ in the SmC slabs is tilted with respect to the axis of the TGB$-C$ helix by an angle ω_L which is roughly equal to the angle between $\mathbf{N}$ and $\mathbf{n}$ (the SmC director tilt angle). $\mathbf{P}_S \propto \mathbf{n} \times \mathbf{N}$ is the polarization and $\hat{\mathbf{x}}$ is the axis of the TGB$_C$ helix (Courtesy: [6]).

Chapter 2

Dislocation arrays in SmA and the structure of TGB$_A$ phase

Accounting for dislocation interactions within covariant linear elasticity theory of SmA, Bluestein *et al.* [4] determined the structural parameters (the spacing l_d of dislocations within grain boundaries and the inter- grain boundary spacing (the smectic block size) l_b) of the TGB$_A$ phase. Their principal result is that the ratio l_b/l_d is close to 0.95 over a wide range of parameter values. In this chapter we show that the structure of the TGB$_A$ phase corresponds to a that of a *triangular reference lattice of screw dislocations* with $l_b/l_d = \sqrt{3/2}$, a result equivalent to that for Abrikosov lattices in conventional superconductors. To address the structure and energetics of the dislocation complexion of TGB$_A$ phase we (*i*) review the energetics of single screw dislocations (Fig. 2.1(a)) in SmA, (*ii*) discuss the topology and geometry of dislocation arrays and show that certain planar dislocation arrays composed of parallel dislocations do not constitute grain boundaries, (*iii*) use the method developed in (*i*) above to obtain the energy per unit area of small-angle twist grain boundaries composed of screw dislocations (Fig. 2.6), (*iv*) evaluate the interaction potential for small-angle twist grain boundaries (Fig. 2.8), and (*v*) elucidate the structure of the TGB$_A$ phase (Figs. 2.11 and 2.12). Our analysis is applicable near the lower critical chiral field.

2.1 Energetics of a single screw dislocation in SmA

In type-II SmA, layer distortions are screened by the Frank director. For small distortions the elastic free energy is

$$F = \int f \, \mathrm{d}^3x = \frac{1}{2} \int \left[D \left(\nabla u + \delta \mathbf{n} \right)^2 + K_1 \left(\nabla \cdot \delta \mathbf{n} \right)^2 + K_2 \left(\nabla \times \delta \mathbf{n} \right)^2 \right] \mathrm{d}^3x, \tag{2.1}$$

where u is the displacement field, $\delta \mathbf{n}$ is the deviation of the Frank director from its undistorted equilibrium value $\mathbf{n}_0 = \mathbf{e}_z$, and D, K_1, and K_2 are elastic constants (we have set the twist elastic constant equal to the bend elastic constant). The Euler-Lagrange equations corresponding to the free energy Eq. (2.1) are

$$\begin{aligned} \frac{\delta F}{\delta u} &= -D \, \nabla \cdot \left(\nabla u + \delta \mathbf{n} \right) = 0, \\ \frac{\delta F}{\delta \mathbf{n}} &= D \left(\nabla u + \delta \mathbf{n} \right) - K_1 \nabla (\nabla \cdot \delta \mathbf{n}) + K_2 \nabla \times \nabla \times \delta \mathbf{n} = 0. \end{aligned} \tag{2.2}$$

In the presence of dislocations, the displacement field is continuous but multivalued. For a screw dislocation (core along $\mathbf{e}_z$) the singular (topological) part of the displacement field is

$$u_\mathrm{s}(\mathbf{x}) = \frac{d}{2\pi} \phi = \frac{d}{2\pi} \arctan \frac{y}{x}, \tag{2.3}$$

where d is the magnitude of the Burgers vector (Fig. 2.1).

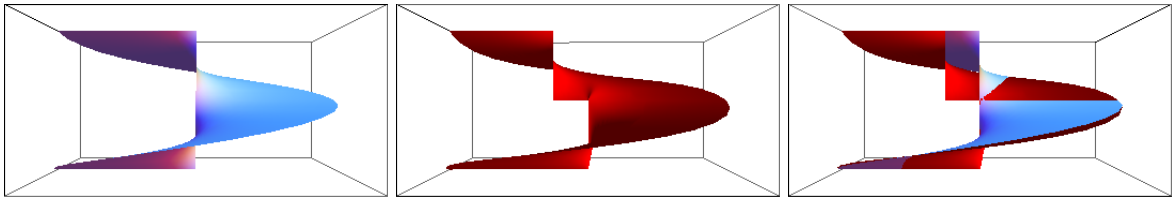

(a) Screw dislocation (b) Mixed dislocation (c) Screw and mixed dislocations: a comparison

Figure 2.1: Schematics of screw (blue) and mixed (red) dislocations. The mixed dislocation line (the core) is tilted by $\pi/4$ with respect to the equilibrium layer normal.

For any loop enclosing the dislocation core $\oint \mathrm{d}u_\mathrm{s} = d$. We treat u_s as a single-valued field which is discontinuous across a cut surface containing the dislocation line. There is no topological constraint on the $\delta \mathbf{n}$ field. The $\delta \mathbf{n}$- field merely adjusts itself to lower the dislocation energy by screening the topologically constrained displacement field. For a screw dislocation the u- and

$\delta\mathbf{n}$- fields satisfying the Euler-Lagrange equations Eq. (2.2) are given by [1]

$$\begin{aligned} u(\mathbf{x}) = u_{\mathrm{s}}(\mathbf{x}) &= \frac{d}{2\pi} \arctan \frac{y}{x}, \\ \delta\mathbf{n}(\mathbf{x}) &= \frac{d}{2\pi} \left[\frac{1}{\lambda_2} K_1 \left(\frac{\rho}{\lambda_2} \right) - \frac{1}{\rho} \right] \mathbf{e}_\phi, \end{aligned} \tag{2.4}$$

where $\rho = \sqrt{x^2 + y^2}$, $\mathbf{e}_\phi$ is the unit vector in the ϕ- direction, λ_2 is the twist penetration depth and $K_1(\rho/\lambda_2)$ in the modified type-II Bessel function of order one. Note that (*i*) the singular part of the displacement field is the solution to the Euler-Lagrange equation, and (*ii*) the $\delta\mathbf{n}$- field is divergence-free.

We use the standard technique for calculating the energy of topological defects [1] and write the free energy density f as

$$\begin{aligned} f = \frac{1}{2}[& D \left\{ \nabla_i (u(\nabla_i u + \delta n_i)) - u \nabla_i (\nabla_i u + \delta n_i) + \delta n_i (\nabla_i u + \delta n_i) \right\} \\ & + K_1 \left\{ \nabla_i (\delta n_i \nabla_j \delta n_j) - \delta n_i (\nabla_i \nabla_j \delta n_j) \right\} \\ & + K_2 \left\{ \epsilon_{ijk} \nabla_j (\delta n_k \, \epsilon_{ipq} \nabla_p \delta n_q) + \delta n_i (\epsilon_{ijk} \epsilon_{kpq} \nabla_j \nabla_p \delta n_q) \right\}], \end{aligned} \tag{2.5}$$

where ϵ_{ijk} is the completely antisymmetric Levi-Civita symbol, and repeated indices are summed over.

Applying Gauss's theorem and using the Euler-Lagrange equations (2.2), the elastic free energy can be recast as

$$\begin{aligned} F &= \frac{D}{2} \int_S (\nabla_i u + \delta n_i) u \, \mathrm{d}S_i \\ &= \frac{D}{2} \int_C (\nabla u + \delta\mathbf{n}) \cdot (\mathbf{N}^+ u^+ + \mathbf{N}^- u^-) \, L \, \mathrm{d}l \\ &= \frac{D}{2} \int (\nabla_i u + \delta n_i) N_i (u^+ - u^-) \, L \, \mathrm{d}x, \end{aligned} \tag{2.6}$$

where C is the cut line, N_i represent the components of the normal vector on the lips of the cut line (Fig. 2.2). $d = (u^+ - u^-)$ is the magnitude of the Burgers vector, and L is the length of the dislocation line. It is convenient to define $\mathbf{Q} = \nabla u + \delta\mathbf{n}$. In particular, the energy per unit length for a single screw dislocation is then given by

$$\left(\frac{F}{L} \right) = \frac{Dd}{2} \int_\xi^\infty Q_y \, \mathrm{d}x, \tag{2.7}$$

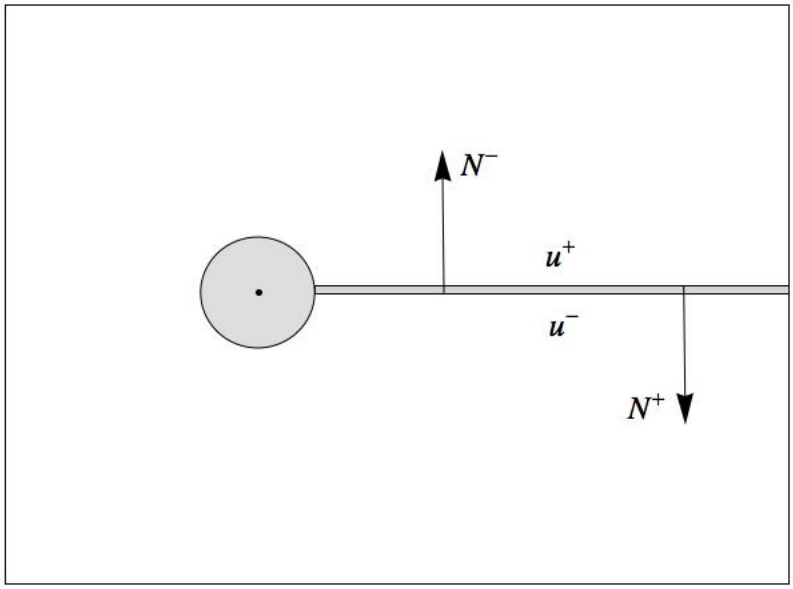

Figure 2.2: The cut line for the calculation of the elastic energy of a single screw dislocation in SmA. $\mathbf{N}^+$ and $\mathbf{N}^-$ are the normals to the two lips of the cut line. u^+ and u^- are the displacement fields on either side of the cut line.

where ξ is the smectic correlation length and the cut line is chosen to be along the x- axis. Here we have ignored the contribution from the dislocation core energy which arises from the destruction of smectic order within a region of order of the smectic correlation length ξ. Using Eq. (2.5) the energy per unit length of a single screw dislocation is [1]

$$\left(\frac{F}{L_z}\right) = \frac{Dd^2}{4\pi} K_0\left(\frac{\xi}{\lambda_2}\right), \tag{2.8}$$

where $K_0(\xi/\lambda_2)$ is the modified type-II Bessel function of order zero and $\lambda_2^2 = K_2/D$. This result is analogous to that for the energy per unit length of a flux tube in type-II superconductors. For small arguments $K_0(\xi/\lambda_2) \approx -\ln(\xi/\lambda_2)$ and we regain the approximate result for the energy of a screw dislocation in a type-II SmA

$$\left(\frac{F}{L_z}\right) = \frac{Dd^2}{4\pi} \ln\left(\frac{\lambda_2}{\xi}\right). \tag{2.9}$$

We note that Eq. (2.6) applies to a general (mixed) straight dislocation line (see Fig. 2.1(b)) In the later sections, we use this formula for calculating the energy per unit area of grain boundaries, and the interaction potential of a grain boundary with a single dislocation.

2.2 Geometry and topology of some dislocation arrays in smectics

As discussed in Chapter 1, small angle grain boundaries can be modelled as arrays of dislocation lines. In this section we obtain the singular, *topological part* of the displacement field for planar arrays of straight, equidistant, edge- and mixed dislocation lines to show that certain arrays do not qualify as small-grain boundaries.

2.2.1 Twist grain boundary

A twist grain boundary in smectics [1, 17] is composed of a planar array of screw dislocations with inter-dislocation spacing l_d, which we take to be along $\mathbf{e}_y$ (Fig. 2.3). The displacement field for this array of dislocations is

$$u^{(\mathrm{tw})}(\mathbf{x}) = \frac{d}{2\pi} \sum_{m=-\infty}^{\infty} \arctan\left(\frac{y - m l_d}{x}\right), \tag{2.10}$$

where the sum is over integers. It is simpler to sum the components of the gradient of the displacement field (which gives the slope of the smectic layers) using the Poisson summation formula (or other methods of complex analysis). The components of $\mathbf{v}^{(\mathrm{tw})}(\mathbf{x}) = \nabla u^{(\mathrm{tw})}(\mathbf{x})$ for a twist grain boundary are [4]

$$\begin{aligned} v_x^{(\mathrm{tw})}(\mathbf{x}) &= -\frac{d}{2l_d} \frac{\sin(2\pi y/l_d)}{\cosh(2\pi x/l_d) - \cos(2\pi y/l_d)}, \\ v_y^{(\mathrm{tw})}(\mathbf{x}) &= \quad \frac{d}{2l_d} \frac{\sinh(2\pi x/l_d)}{\cosh(2\pi x/l_d) - \cos(2\pi y/l_d)}, \end{aligned} \tag{2.11}$$

with the limiting form for large $|x|$ given by $\mathbf{v}^{(\mathrm{tw})}(x \to \pm\infty) = \pm(d/(2l_d))\,\mathbf{e}_y$. At large $|x|$ the layers undergo a pure rotation across the array. This array qualifies as a twist grain boundary.

Notice that $v_y^{(\mathrm{tw})}(\mathbf{x})$ and $v_x^{(\mathrm{tw})}(\mathbf{x})$ are respectively the real and imaginary parts of the function

$$f(\zeta) = \frac{d}{2\pi} \frac{\pi}{l_d} \coth\left(\frac{\pi\zeta}{l_d}\right) = \frac{d}{2\pi} \frac{\mathrm{d}}{\mathrm{d}\zeta} \ln\sinh\left(\frac{\pi\zeta}{l_d}\right) \tag{2.12}$$

of the complex variable $\zeta = x + iy$. The function $\pi\coth(\pi\zeta)$ has simple poles with unit residue at all integers along the imaginary axis. Since $\mathrm{Arg}[\ln\sinh(\zeta)] = \tan y/\tanh x$, the displacement

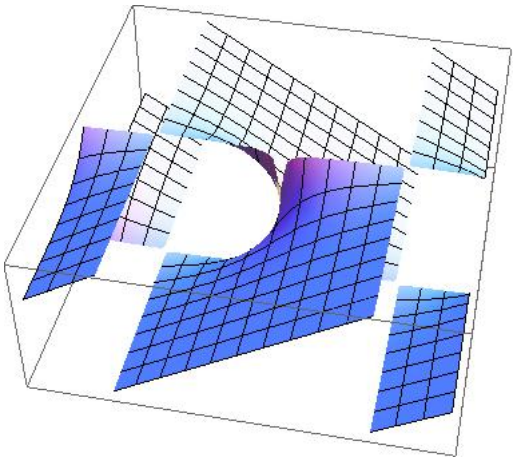

Figure 2.3: Close-up of a twist grain boundary generated using Eq. (2.13) (see text).

field for a twist grain boundary is

$$u^{(\mathrm{tw})}(\mathbf{x}) = \frac{d}{2\pi} \sum_{m=-\infty}^{\infty} \arctan\left(\frac{y - m l_d}{x}\right) = \frac{d}{2\pi} \arctan\left(\frac{\tan(\pi y/l_d)}{\tanh(\pi x/l_d)}\right). \tag{2.13}$$

2.2.2 A comment on planar arrays of straight dislocation lines

We now consider arrays of edge- and mixed, straight dislocation lines . The form of the displacement field for such dislocation lines is somewhat complicated. For general, mixed dislocation lines the singular "$\arctan$"- form does not satisfy the Euler-Lagrange equation $\delta F/\delta u = 0$, and it is essential to add an analytic part $u_{\mathrm{a}}(\mathbf{x})$ to ensure stability. The displacement field of any straight dislocation line can always be written as $u(\mathbf{x}) = u_{\mathrm{s}}(\mathbf{x}) + u_{\mathrm{a}}(\mathbf{x})$, with $\arctan$- form for the singular part. For screw dislocations in SmA, $u_{\mathrm{a}}(\mathbf{x}) = 0$. To understand the geometry of smectic layers at large distances from planar arrays of parallel, equidistant dislocation lines it is sufficient to consider only the singular part of the displacement field. This is because the topological (singular) part solely determines the deformation (pure rotation, or otherwise) of smectic layers at large distances from a planar dislocation array.

2.2.3 Tilt grain boundary

With $u_{\mathrm{s}}(\mathbf{x}) = (d/(2\pi)) \arctan(y/z)$ for a dislocation with core along the $\mathbf{e}_x$, we set up an array of equidistant (spacing l_d along $\mathbf{e}_y$) edge dislocations. The displacement field for this array can

be read off using Eq. (2.13):

$$u_{\rm s}^{(\rm tl)}(\mathbf{x}) = \frac{d}{2\pi} \arctan \frac{\tan(\pi y/l_d)}{\tanh(\pi z/l_d)}. \tag{2.14}$$

The slopes of the layers $\mathbf{v}^{(\rm tl)}(z \to \pm\infty) = \pm(d/(2l_d))\,\mathbf{e}_y$. At large $|z|$ the layers undergo a pure rotation on both sides of this tilt grain boundary.

2.2.4 An array of edge dislocations

With $u_{\rm s}(\mathbf{x}) = (d/(2\pi))\arctan(z/x)$ for a dislocation with core along $\mathbf{e}_y$, we stack edge dislocation lines along the $\mathbf{e}_z$ direction with inter-dislocation spacing l_d. The singular part of the displacement field for this array is

$$u_{\rm s}^{(\rm e-a)}(\mathbf{x}) = \frac{d}{2\pi} \arctan \frac{\tan(\pi z/l_d)}{\tanh(\pi x/l_d)}. \tag{2.15}$$

The limiting form for large $|x|$ given by $\mathbf{v}^{(\rm e-a)}(x \to \pm\infty) = \mp(d/(2l_d))\,\mathbf{e}_z$. At large $|x|$ the layers do not undergo any rotation, but the layer compression attains a nonzero value. This structure is that of an infinite array of half-layers stacked one on top of the other, which clearly leads to the compression of the layers even at a large distance from the array. This structure is therefore untenable.

2.2.5 Arrays of mixed dislocations

We now consider two types of planar arrays of equidistant mixed dislocation lines. Mixed dislocation lines have the characteristics of screw- as well as edge dislocations. We show here that a certain class of arrays of mixed dislocation lines do not form a grain boundary.

Grain boundary of mixed dislocations

The displacement field of mixed dislocation line tilted in the xz- plane, and passing through the origin has the singular part $u_{\rm s}(\mathbf{x}) = (d/(2\pi))\arctan(y/\tilde{x})$, where $\tilde{x} = x\cos\gamma + z\sin\gamma$. The singular part of the displacement field for a planar array of such dislocation lines with inter-dislocation spacing l_d along $\mathbf{e}_y$ is obtained via the replacement $x \mapsto \tilde{x}$ in the expression Eq. (2.10)

for a twist grain boundary:

$$u_s^{(\mathrm{mx-gb})}(\mathbf{x}) = \frac{d}{2\pi} \arctan\left(\frac{\tan(\pi y/l_d)}{\tanh(\pi \tilde{x}/l_d)}\right) \tag{2.16}$$

The slopes of the layers $\mathbf{v}^{(\mathrm{mx-gb})}(\tilde{x} \to \pm\infty) = \pm(d/(2l_d))\,\mathbf{e}_y$. At large $|\tilde{x}|$ the layers undergo a pure rotation on both sides of this tilt grain boundary. For the special cases $\gamma = 0, \pi$ and $\gamma = \pm\pi/2$, the mixed grain boundary reduces to twist- and tilt grain boundaries respectively.

An array of mixed dislocations

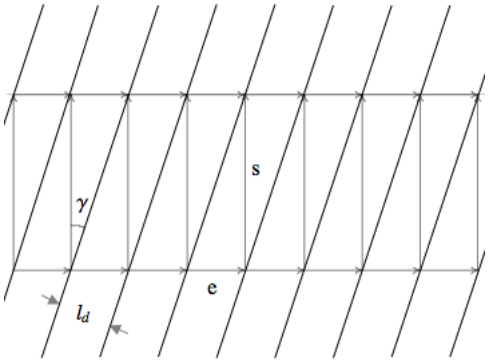

Figure 2.4: Decomposition of the array of mixed dislocation lines into mutually orthogonal screw- ($\mathbf{s}$) and edge ($\mathbf{e}$) lines with Burgers vector $\mathbf{b} = b\mathbf{e}_z$. The black lines represent the tilted dislocation lines, and the grey arrows indicate the separation between edge $l_e \perp \mathbf{b}$, and screw $l_s \parallel \mathbf{b}$ lines.

We now consider an array of mixed dislocations lines that are tilted in the plane of the array. With the replacement $y \mapsto \tilde{y} = y\cos\gamma - z\sin\gamma$, we get

$$u_s^{(\mathrm{mx-a})}(\mathbf{x}) = \frac{d}{2\pi} \arctan\left(\frac{\tan(\pi \tilde{y}/l_d)}{\tanh(\pi x/l_d)}\right) \tag{2.17}$$

for a planar array of mixed dislocation lines with inter-dislocation spacing l_d along $\mathbf{e}_{\tilde{y}}$. Thus the components of the displacement gradient

$$\mathbf{v}^{(\mathrm{mx-a})}(\tilde{x} \to \pm\infty) = (0, \pm\left(\frac{d}{2l_d}\right)\cos\gamma, \pm\left(\frac{d}{2l_d}\right)\sin\gamma). \tag{2.18}$$

In addition to a rotation, the smectic layering attains a nonzero compression at large $|x|$. Note that the dislocation array discussed above can be decomposed into two mutually orthogonal arrays

of pure screw- and edge dislocation lines (Fig. 2.4). The separation between neighbouring edge lines $l_e = l_d/\cos\gamma$, and that between screw lines $l_s = l_d/\sin\gamma$. This array is the superposition of a twist grain boundary and the edge dislocation array (see previous section), and does not qualify as a grain boundary.

2.2.6 Geometry of two twist grain boundaries

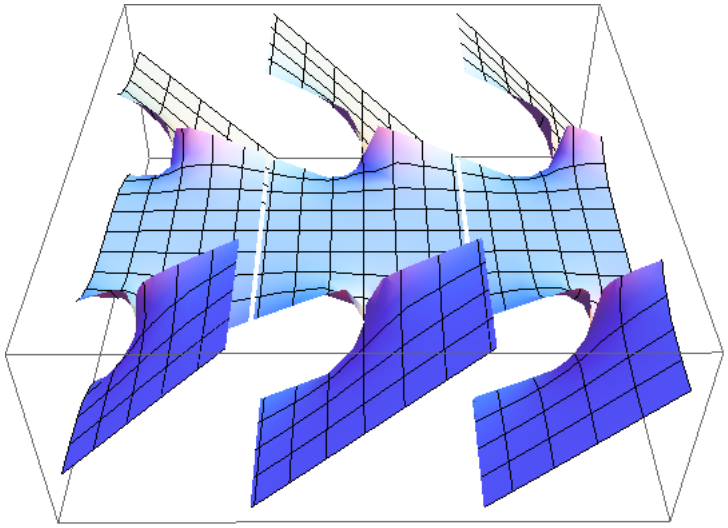

Figure 2.5: Two grain boundaries situated at $x = \pm 7.5\,d$. The dislocation complexion consists of *pure screw dislocations lines parallel to the* z*- axis* placed at $y = 10\,nd\,(l_d = 10d)$, where n is an integer.

The TGB$_A$ structure consists of parallel twist grain boundaries separated by a fixed distance. A proper description of the dislocation complexion of several twist grain boundaries is therefore essential for analysing the geometry as well energetics of the TGB$_A$ phase. In the discussion that follows, we restrict ourselves to small-angle grain boundaries separated by a distance much larger than d, so that linear elasticity and superposition principle are valid. Figure 2.5 shows two twist grain boundaries comprising pure screw dislocations $\mathbf{b} = d\mathbf{e}_z$. *The dislocation sources in both grain boundaries are consistently defined with the same fiducial choice*: $\mathbf{n}_0 = \mathbf{N}_0 = \mathbf{e}_z$. Note that (*i*) as required, this dislocation complexion leads to the correct rotations of smectic blocks obtained via Eq. (2.13), and (*ii*) the dislocation sources retain their character, *i.e.*, have no edge component. In the discussion above, we have seen that arrays of sources with an edge-component lying in the plane of the array do not constitute grain boundaries. The dislocation complexion of TGB$_A$ phase is described in the later sections. The nature of the dislocation

complexion that we use is at variance with that of [4]. In calculating the interaction energy between two grain boundaries, [4] erroneously choose the geometry discussed in the previous section for arrays of mixed dislocation lines which do not form a grain boundary. The only consistent way of calculating interactions between grain boundaries within linear theory is to consider them as being composed of screw dislocation lines in the "reference lattice". This is the geometry we use while calculating the Gibbs free energy for the TGB_A phase, in the later sections.

2.3 Energetics of a Single Twist Grain Boundary

The method described for calculating the elastic energy of a single dislocation line can be extended to evaluate the energy per unit area of a small-angle twist grain boundary. The components of the **Q**- field for a twist grain boundary with dislocation lines along the y- axis are

$$\begin{aligned} Q_x(x,y) &= -\frac{d}{2\pi\lambda}\sum_{m=-\infty}^{\infty}\left(\frac{y_m}{r_m}\right)K_1\left(\frac{r_m}{\lambda}\right), \\ Q_y(x,y) &= \frac{d}{2\pi\lambda}\sum_{m=-\infty}^{\infty}\left(\frac{x}{r_m}\right)K_1\left(\frac{r_m}{\lambda}\right), \end{aligned} \tag{2.19}$$

where $r_m = \sqrt{x^2+y_m^2}$, $y_m = (y - ml_d)$, and we have set $\lambda = \lambda_2$ to simplify notation.

The elastic energy per unit area of a single twist grain boundary is

$$\begin{aligned} E/A &= \frac{Dd}{2}\lim_{L_y\to\infty}\frac{1}{L_y}\sum_{m=-\infty}^{\infty}\int_{C_m} Q_y(x,y_m)\,d\,\mathrm{d}x \\ &= \frac{Dd}{2}\frac{d}{l_d}\int_{x_0}^{\infty}\sum_{m=-\infty}^{\infty} Q_y(x,ml_d)\,\mathrm{d}x \\ &= \frac{Dd}{4\pi}\frac{d}{l_d}\sum_{m=-\infty}^{\infty}K_0\left(\frac{\rho_m}{\lambda}\right), \end{aligned} \tag{2.20}$$

where L_y is the length of the grain boundary, C_m are cut- planes $y = ml_d$, x_0 (which we set equal to ξ, see below) is the lower limit of integration, and $\rho_m = \sqrt{x_0^2 + (ml_d)^2}$. It should be noted that in the above expression we have neglected the contribution from the core energy of dislocations.

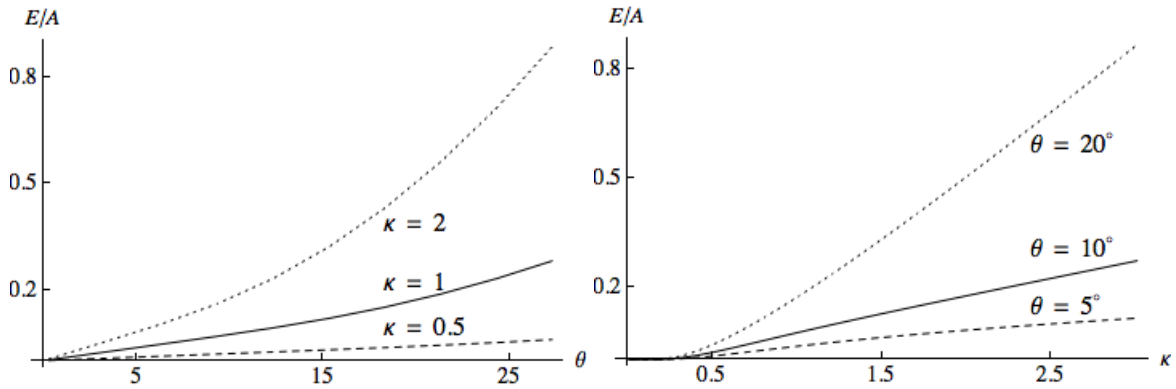

(a) E/A as a function of θ (in degrees), for $\kappa = 0.5$ (dashed), 1 (continuous), and 2 (dotted).

(b) E/A as a function of κ, for $\theta = 5$ (dashed), 10 (continuous), and 20 (dotted) degrees.

Figure 2.6: Energy per unit area E/A of twist grain boundaries (in units of $Dd/(4\pi)$)

To evaluate the sum in Eq. (2.20) above, we use the integral representation (see [39])

$$K_0(z) = \frac{1}{2}\int_0^\infty \frac{e^{-t}}{t} e^{-z^2/(4t)}\,\mathrm{d}t, \tag{2.21}$$

and the identity

$$\sum_{m=-\infty}^{\infty} \exp[(x-m)^2] = \sqrt{\pi}\,\vartheta_3(-\pi x, \exp[-\pi^2]), \tag{2.22}$$

where $\vartheta_3(z,q)$ represents the type-III theta function with nome q (the identity follows from the definition of $\vartheta_3(z,q)$, see [40]). With $z = r_m/\lambda$ the energy per unit area Eq. (2.20) is

$$E/A = \frac{Dd}{4\pi}\frac{d}{l_d}\frac{\lambda}{l_d}\int_0^\infty \sqrt{\frac{\pi}{t}}\,\exp\left[-t - \frac{(\xi/\lambda)^2}{4t}\right]\,\vartheta_3(-\pi(y/l_d),\,\exp[-4\pi^2\,(\lambda/l_d)^2\,t])\,\mathrm{d}t, \tag{2.23}$$

where, as in Eq. (2.20), we have used the smectic correlation length ξ as the lower cutoff. Setting $y = 0$, $\kappa = \lambda/\xi$, $\xi \simeq d$, and $\theta = d/l_d$ gives

$$E/A = \frac{Dd}{4\pi}\kappa\,\theta^2\int_0^\infty \sqrt{\frac{\pi}{t}}\,\exp\left[-t - \frac{1}{4\kappa^2 t}\right]\,\vartheta_3(0,\,\exp[-4\pi^2\,\kappa^2\theta^2\,t])\,\mathrm{d}t. \tag{2.24}$$

The elastic energy per unit area of twist grain boundaries as functions of the grain boundary angle θ and κ are plotted in (Fig. 2.6).

For small θ, Eq. (2.24) reduces to

$$E/A \approx \frac{Dd}{4\pi}\,\theta \int_0^\infty \frac{1}{t} \exp\left[-t - \frac{1}{4\kappa^2 t}\right] \left(\frac{1}{2} + \exp\left[-\frac{1}{4\kappa^2\theta^2 t}\right]\right) \mathrm{d}t$$
$$= \frac{Dd}{4\pi}\,\theta \left(K_0(1/\kappa) + \sqrt{2\pi\,\kappa\,\theta}\,\exp[-1/(\kappa\,\theta)]\right), \tag{2.25}$$

where we have extracted the asymptotic behaviour of $\vartheta_3(0,\, \exp(-4\pi^2\,\kappa^2\theta^2\,t))$. (Fig. 2.7) compares Eq. (2.25) to the exact result Eq. (2.24).

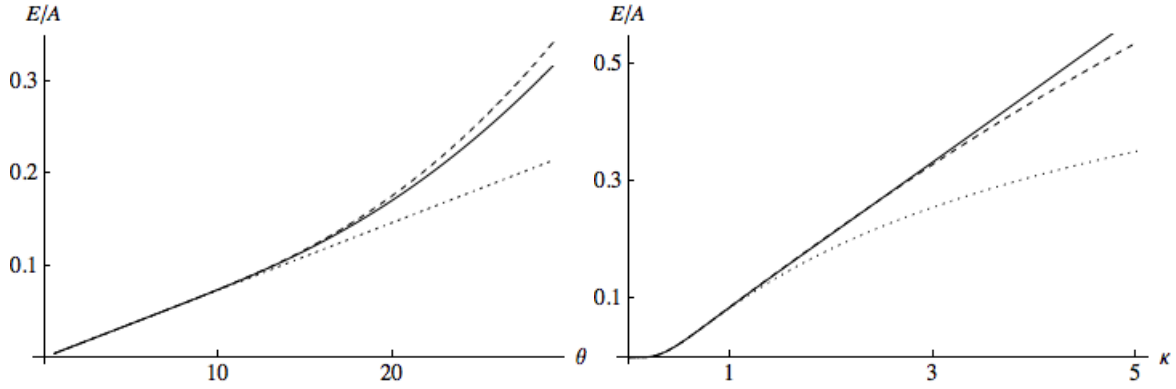

Figure 2.7: Approximations to E/A (in units of $Dd/(4\pi)$), θ in degrees. Exact result Eq. (2.24)(continuous), linear approximation from Eq. (2.25) (dotted), the full expression Eq. (2.25) (dashed). (a) $\kappa = 1$, (b) $\theta \simeq 12^\circ$.

For small angle grain boundaries, the contribution to the energy per unit area from the core energy is proportional to θ. Including this contribution gives the total energy per unit area of a twist grain boundary

$$\mathcal{E}/A = A\,\theta + \frac{Dd}{4\pi}\,\theta \left(K_0(1/\kappa) + \sqrt{2\pi\,\kappa\,\theta}\,\exp[-1/(\kappa\,\theta)]\right), \tag{2.26}$$

where we have introduced a phenomenological parameter A to account for the core energy of dislocation lines arising from destruction of smectic order.

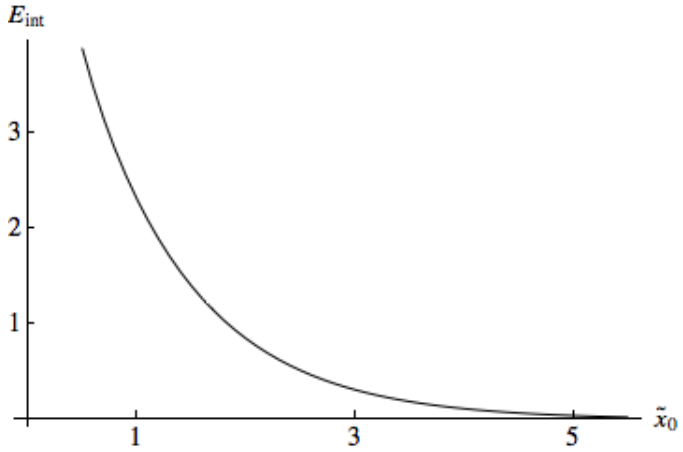

(a) E_{int} as a function of $\tilde{x}_0 = x_0/l_d$.

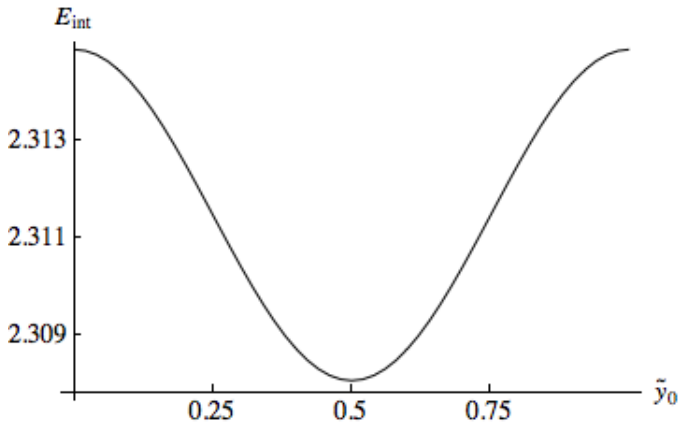

(b) E_{int} as a function of $\tilde{y}_0 = y/l_d$ for $\tilde{x}_0 = 1$.

Figure 2.8: E_{int} (in units of $Dd/(4\pi)$) between a twist grain boundary and a screw dislocation.

2.4 Interaction of a twist grain boundary with a single screw dislocation

The interaction energy per unit length of a screw single dislocation situated at (x_0, y_0) with a twist grain boundary with screw dislocations at $x = 0$, $y = nl_d$ is

$$E_{\text{int}} = \frac{Dd^2}{4\pi}\left(\frac{\lambda}{l_d}\right)\int_0^\infty \sqrt{\frac{\pi}{t}}\,\exp\left(-t - \frac{x_0^2}{4\lambda^2 t}\right)\,\vartheta_3(-\pi(y_0/l_d),\,\exp(-4\pi^2\,(\lambda/l_d)^2\,t))\,\mathrm{d}t. \tag{2.27}$$

We evaluate this integral numerically (Fig. 2.8). We find that the interaction energy is minimum for a dislocation which is situated mid-way between grain boundary dislocations (at $y = ml_d/2$) for any x_0.

This result suggests that the TGB$_A$ lattice may correspond to a *triangular reference lattice* in the sense discussed in the following section.

2.5 Geometry of the TGB$_A$ phase

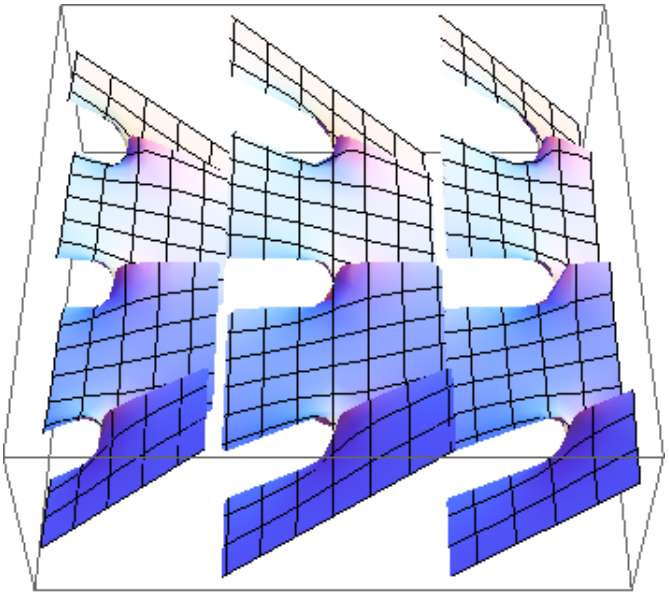

Figure 2.9: Smectic layering for TGB$_A$ structure that corresponds to a square reference lattice . For clarity, only one layer is shown for each block.

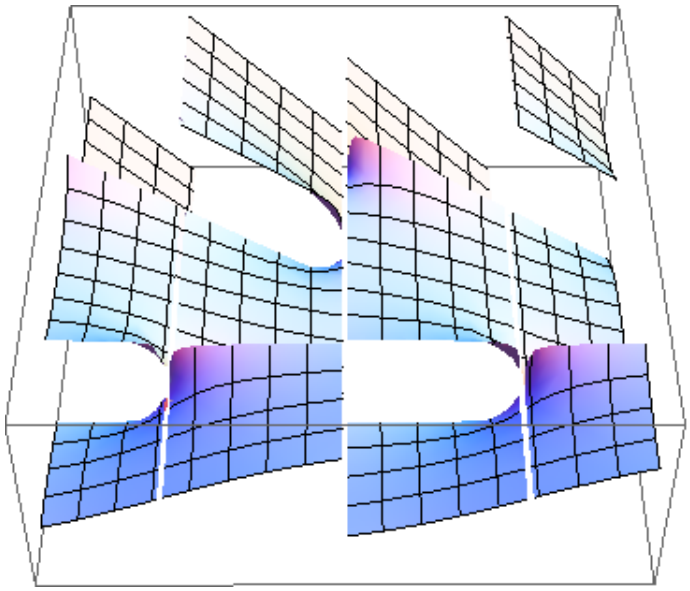

Figure 2.10: Smectic layering in a "unit reference cell" of triangular TGB$_A$ structure.

Let us construct a dislocation complexion by placing screw dislocations with Burgers vectors $d\,\mathbf{e}_z$ at $x = m\,l_b,\ y = n\,l_d$, where m, n are integers (Fig. 2.9). We note that in this complexion all the dislocation lines are parallel to each other. In terms of the displacement fields of single grain boundaries, the displacement field is

$$U(\mathbf{x}) = \frac{d}{2\pi} \sum_{m=-\infty}^{\infty} \arctan\left(\frac{\tan(\pi y/l_d)}{\tanh(\pi(x - m\,l_b)/l_d)}\right). \tag{2.28}$$

For the displacement field given above, the layer normals evaluated at $x = (p + (1/2))\,l_b$ have components $-\nabla_x U(\mathbf{x}) = 0,\ -\nabla_y U(\mathbf{x}) = (2p+1)\,d/(2l_d))$ for integer values of p, as expected from the TGB$_A$ structure. This complexion comprises a rectangular *reference lattice* of parallel screw dislocations with lattice parameters l_b, l_d. In real space, the smectic layers themselves rotate from one grain to the next, but the dislocation lines in each grain boundary are screw dislocations (since they are oriented along the local layer normal). Therefore, within linear theory, their interaction energies will be that between parallel screw dislocation lines, even though in real space, they may be rotated with respect to each other. The smectic layering for a triangular reference lattice of screw dislocations is shown in Fig. 2.10. In general, any oblique lattice of parallel screw dislocations qualifies for the TGB$_A$ structure.

2.6 Energetics of the TGB$_A$ phase

The presence of molecular chirality introduces an additional term in the free energy, of the form $-h \int \mathrm{d}^3x\ \mathbf{n} \cdot (\nabla \times \mathbf{n})$. In the presence of a chiral field, the smectic phase may become unstable to the formation of the twist grain boundary phase. The average chiral energy per unit volume is given by $h\,d/l_b l_d$ [1]. The Gibbs free energy per unit volume of the TGB$_A$ phase in the presence of a chiral field h is obtained by subtracting the chiral energy per unit volume from the energy per unit volume (obtained via Eqs. 2.24 and 2.27) of the lattice of screw dislocation lines defined in Section 2.5.

$$\frac{G_{\mathrm{tgb}}}{V} = \frac{F_{\mathrm{lattice}}}{V} - \frac{hd}{l_b l_d}. \tag{2.29}$$

We numerically minimize the Gibbs free energy G_{tgb} per unit volume for rectangular as well as triangular reference lattices. Our results are summarized in Fig. 2.11 and Fig. 2.12.

Figure 2.11 shows the variation of the lattice parameters for a rectangular reference lattice (lattice parameters l_b and l_d), and a triangular reference lattice (lattice parameter a), as a function of $hd - E$. Here, h is the chiral field, d is the layer spacing (the Burgers vector of a single dislocation line) and E is the elastic energy cost of creating a single screw dislocation line. The plot shows that for the rectangular lattice that minimizes the Gibbs free energy, the one with $l_b = l_d$ (a square lattice) has the lowest energy.

Figure 2.12 shows the *difference* in the Gibbs free energy per volume as a function of $hd - E$. The difference is positive, indicating that the triangular reference lattice constitutes the minimum energy TGB$_A$ structure, rather than the square reference lattice.

In conclusion, we emphasize the major differences in the treatment of [4] to that discussed in this chapter: (*i*) In Section 2.2.5, we have shown that an array or mixed dislocations which are tilted in the plane of the array, do not form a grain boundary. The dislocation complexion of [4] involves arrays of this kind. (*ii*) We use the full interaction potential (Eq. (2.27)) as against the exponentially decaying potential used by [4].

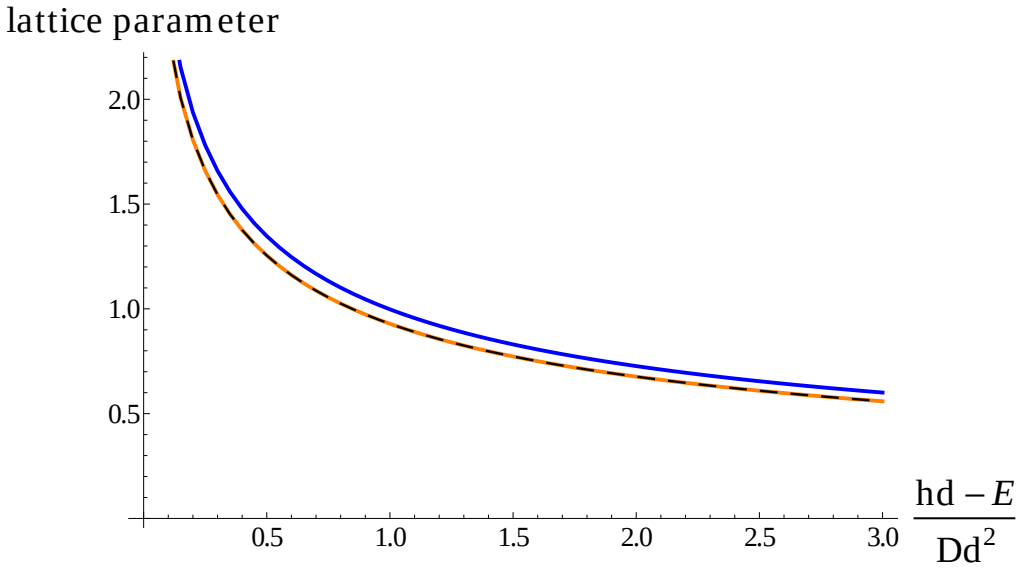

Figure 2.11: The lattice parameters (l_b (orange) and l_d (dashed) for the rectangular lattice, and a (blue) for the triangular lattice) in the minimum energy reference lattice, as a function of $(h\,d - E)/D\,d^2$, in the TGB$_A$ phase. For the rectangular lattice, the Gibbs free energy is minimized when $l_b = l_d$ (the square lattice). Distances are measured in units of λ.

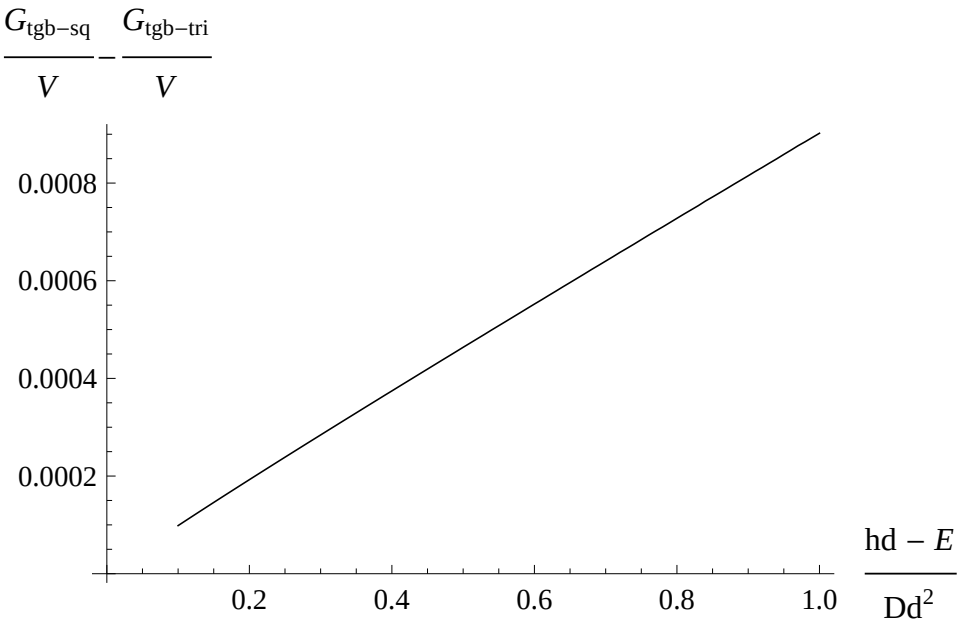

Figure 2.12: The *difference* of the Gibbs free energy per unit volume(measured in units of Dd^2/λ^2) between a square lattice and a triangular lattice, as a function of $(h\,d - E)/Dd^2$. The difference is positive, indicating that a square lattice has a greater Gibbs free energy than a triangular lattice, for the same value of the chiral field h.

Chapter 3

An instability in SmC: The modulated phase

3.1 Introduction

Covariant elasticity theories of smectics are obtained as "low-temperature" limits (in which the modulus of the complex order parameter is fixed) of the Ginzburg-Landau-de Gennes theory [1, 14]. In the context of type-II chiral smectogens, theoretical investigations of TGB phases rely on such covariant formulations of free energy [5, 17]. *TGB phases are not feasible in achiral materials, even if they are type-II in character*. We propose a modulated instability which is a manifestation of covariance in the unusual setting of *achiral* SmC materials. We show that the linear, covariant elasticity theory of SmC [18] (introduced in Section 1.3) admits a transition to a modulated structure with an oblique wavevector (in the xz- plane) as the ground state of the smectic medium (see Fig. 3.3). Tilt order, the distinctive feature of SmC, introduces new elastic couplings (that are absent in SmA) in the covariant elasticity theory. Modulated instability sets in if the elastic constants discussed below satisfy the inequality $L^2 > B\,D$. Here B is the layer compression modulus, D is the coefficient of the covariant term which ensures that deviations from simultaneous, global rigid rotations of the layer normal with the Frank director cost energy, and L is the coefficient of the term that couples these two distortions in the elastic free energy (see the discussion following Eq. (3.4)). Tilt order is essential for the instability; symmetry of SmA prohibits a term analogous to the L- term in the elastic free energy. Previous formulations of SmC elasticity, coupling molecular tilt to layer displacement (see, *e.g.*, [10]), do not lead to the instability discussed here. We point out that an earlier observation of a periodic pattern in a SmC material [7] is consistent with the predicted structure.

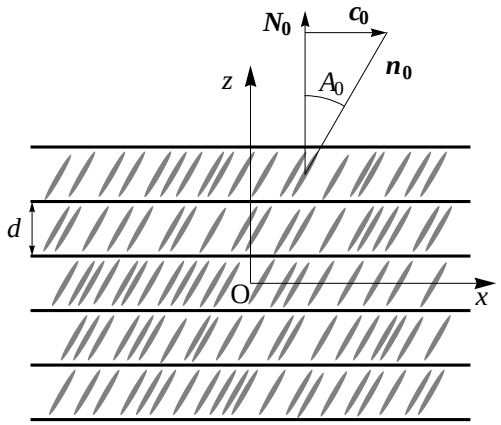

Figure 3.1: Schematic of SmC. The xz- plane is a mirror plane and O is a point of inversion. $\mathbf{n}_0 \equiv -\mathbf{n}_0$ is the unit Frank director, and the unit layer normal $\mathbf{N}_0$ is along the z-axis. The polar vector $\mathbf{c}_0 = (c_0, 0, 0)$ is the projection of $\mathbf{n}_0$ onto the plane of the layers. The equilibrium layer spacing is d. In SmA, $\angle A_0 = 0$ and the layered structure is uniaxial.

3.2 The elastic free energy: stability analysis

SmC is a biaxial phase (Fig. 3.1) in which the molecular director $\mathbf{n}_0$ is tilted with respect to the layer normal $\mathbf{N}_0$ so that $\mathbf{n}_0 \cdot \mathbf{N}_0 = \cos A_0 \equiv \alpha$. The projection of the Frank director onto the layers is denoted by $\mathbf{c}_0$. The plane spanned by $\mathbf{n}_0$ and $\mathbf{N}_0$ is a mirror plane with a centre of inversion, and the structure is invariant under the simultaneous transformation $\mathbf{N}_0 \to -\mathbf{N}_0$, $\mathbf{c}_0 \to -\mathbf{c}_0$. In the distorted SmC the director

$$\mathbf{n} = \mathbf{n}_0 + \delta\mathbf{n} = \mathbf{c} + \sqrt{1 - c^2}\ \mathbf{N}, \tag{3.1}$$

where $\mathbf{c} = (c_0 + \delta c)(\cos\phi, \sin\phi, 0)$, δc is the change in the magnitude of $\mathbf{c}$, and ϕ is the azimuthal angle. To the lowest order, the distortion in the director field is

$$\delta\mathbf{n} \simeq \left(\delta c,\ c_0\,\delta\phi,\ -c_0\,\delta c/\sqrt{1 - c_0^2}\right), \tag{3.2}$$

and the distorted layer normal is given by

$$\mathbf{N} \simeq (-\partial_x u, -\partial_y u, 1), \tag{3.3}$$

where the field $u(\mathbf{x}) = u(x, y, z)$ measures the displacement of layers along the z- direction.

The broken symmetry elastic variables are $u(\mathbf{x})$, $\delta c(\mathbf{x})$ and $\delta\phi(\mathbf{x})$. The covariant, harmonic elastic free energy density is [18]

$$f = (1/2)\,[B\,(\partial_z u)^2 + D\,(\delta c + \alpha\,\partial_x u)^2 - 2L\,(\delta c + \alpha\,\partial_x u)(\partial_z u) + K_u\,(\nabla^2 u)^2 + K_c\,(\nabla\delta c)^2 + K_\phi\,(\nabla\delta\phi)^2], \tag{3.4}$$

with the elastic free energy functional given by $F[u(\mathbf{x}), \delta c(\mathbf{x}), \delta\phi(\mathbf{x})] = \int f\,\mathrm{d}^3x$. The terms with coefficients B and K_u account for layer- compression and layer- bend energies respectively. In principle, the symmetry of SmC allows for anisotropy in the bend modulus. In Eq. (3.4) above, the anisotropy in the effective bend modulus is taken into account indirectly via the coupling to the δc- field (see [18] for a detailed discussion). The Frank free energy for distortions in the director field is represented via terms with coefficients K_c and K_ϕ in the one-constant approximation [10]. The D- and L- terms involve the form $(\delta c + \alpha\,\partial_x u)$ which measures the deviation $\delta(\mathbf{n}\cdot\mathbf{N}) = \mathbf{n}_0\cdot\delta\mathbf{N} + \delta\mathbf{n}\cdot\mathbf{N}_0$ from its equilibrium value α. For simultaneous, rigid rotations of the Frank director and the layer normal, $\delta(\mathbf{n}\cdot\mathbf{N}) = 0$. The term with the coefficient L is allowed by the symmetry of SmC, and couples $\delta(\mathbf{n}\cdot\mathbf{N})$ to changes in the equilibrium layer spacing. This term is crucial for the proposed instability, and has no counterpart in the covariant elasticity theory of SmA [1]. The elastic constants B, D, K_u, K_c and K_ϕ have to be positive for stability. Stability conditions do not restrict the sign of L. Notice that the B-, D-, and L terms involve only x- and z- gradients of the broken symmetry variables. Furthermore, the $\delta\phi$- field is not coupled to the u- and δc- fields. The term with coefficient K_ϕ plays no role in the modulated instability presented in this chapter (see the discussion following Eq. (3.15)), and will be ignored in the following analysis.

We now recast the elastic free energy in a form which is suited for the analysis of the proposed instability. In Fourier space the elastic free energy can be expressed as

$$F = \frac{1}{2}\int \frac{\mathrm{d}^3q}{(2\pi)^3}\,\Phi_a^*(\mathbf{q})\,G_{ab}^{-1}(\mathbf{q})\,\Phi_b(\mathbf{q}), \tag{3.5}$$

where repeated indices are summed over, $\Phi_1(\mathbf{q}) = u(\mathbf{q})$, $\Phi_2(\mathbf{q}) = \delta c(\mathbf{q})$, and

$$\begin{aligned} G_{11}^{-1}(\mathbf{q}) &= B\,q_z^2 + \alpha^2 D\,q_x^2 - 2\alpha L\,q_x q_z + K_u\,q^4, \\ G_{12}^{-1}(\mathbf{q}) &= -\,G_{21}^{-1}(\mathbf{q}) = i\,(L\,q_z - \alpha D\,q_x), \\ G_{22}^{-1}(\mathbf{q}) &= D + K_c\,q^2. \end{aligned} \tag{3.6}$$

The Euler-Lagrange equations are

$$\frac{\delta F}{\delta \phi_a^*(\mathbf{q})} = G_{ab}^{-1}(\mathbf{q})\,\phi_b(\mathbf{q}) = 0; \tag{3.7}$$

in particular, setting $\delta F/\delta c(-\mathbf{q}) = 0$ gives

$$\delta c(\mathbf{q}) = \, i\,\frac{(L\,q_z - \alpha D\,q_x)}{D + K_c\,q^2}\,u(\mathbf{q}). \tag{3.8}$$

Using Eq. (3.8) to eliminate the δc- field from the free energy (Eq. (3.5)) leads to the effective free energy as a functional of the u- field alone -

$$F_{\rm eff}[u] = \frac{1}{2}\,\frac{B}{\xi^5}\int \frac{{\rm d}^3p}{(2\pi)^3}\,\frac{g(\mathbf{p})}{1+\kappa_c^2\,p^2}\,u(\mathbf{p})u(-\mathbf{p}), \tag{3.9}$$

where the dimensionless wavevector $\mathbf{p} \equiv \mathbf{q}\,\xi$, and the anisotropic function $g(\mathbf{p})$ is described in Eqs. (3.10) and (3.11) below. In order to simplify the discussion of stability conditions we have introduced the rescaled dimensionless parameters $l_B = \alpha L/B, d_B = \sqrt{\alpha^2 D/B}, \kappa_u = \lambda_u/\xi, \kappa_c = \lambda_c/\xi$, and the lengths $\lambda_u = \sqrt{K_u/B},\ \lambda_c = \sqrt{K_c/D}$. In terms of these parameters

$$g(\mathbf{p}) = g_2(\mathbf{p}) + g_4(\mathbf{p}) + g_6(\mathbf{p}), \tag{3.10}$$

where

$$\begin{aligned} g_2(\mathbf{p}) &= [1-(l_B/d_B)^2]\,p_z^2, \\ g_4(\mathbf{p}) &= [\kappa_u^2\,p^2 + \kappa_c^2\{(p_z - d_B p_x)^2 + 2(d_B - l_B)p_x p_z\}]p^2, \\ g_6(\mathbf{p}) &= \kappa_u^2\,\kappa_c^2\,p^6. \end{aligned} \tag{3.11}$$

Thus any equilibrium configuration has to satisfy the condition $\delta F_{\rm eff}/\delta u(-\mathbf{p}) = 0$, which gives

$$\frac{g(\mathbf{p})}{1+\kappa_c^2\,p^2}\,u(\mathbf{p}) = 0. \tag{3.12}$$

The denominator of the Euler-Lagrange equation (3.12) is positive. Therefore it is sufficient to consider the algebraic equation $g(\mathbf{p})\,u(\mathbf{p}) = 0$ in analysing the stability of the SmC phase. Notice that for the terms constituting $g(\mathbf{p})$ the inequalities
(*i*) $g_2(\mathbf{p}) > 0$ if $l_B^2 < d_B^2$, that is, $L^2 < BD$,
(*ii*) $g_4(\mathbf{p}) > 0$ if $l_B^2 < (d_B^2 + (\kappa_u/\kappa_c)^2)(1 + (\kappa_u/\kappa_c)^2)$, and

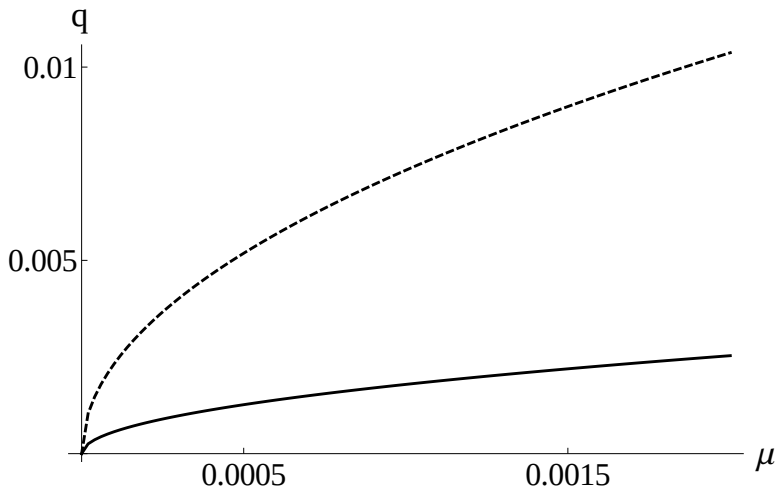

Figure 3.2: The components of modulation wave-vector (measured in units of ξ^{-1}), q_x (continuous) and q_z (dashed), as functions of $\mu \equiv (l_B^2/d_B^2 - 1)$, for $\kappa_c = 3$, $\kappa_u = 1$ and $d_B = 1/3$.

(*iii*) $g_6(\mathbf{p}) > 0$ hold for all $\mathbf{p}$.

The above inequalities ensure that that the Euler-Lagrange equation (3.12) is satisfied only for $\mathbf{p} = 0$, which corresponds to the SmC ground state. Condition (*ii*) is always satisfied if the inequality for the elastic coefficients in (*i*) holds. If condition (*i*) does not hold, *i.e.*, if $L^2 > B\,D$, and if $g_4(\mathbf{p}) > 0$, the equation for stability Eq. (3.12) has solutions $u(\mathbf{p})$ with nonzero $\mathbf{p}$. Thus the range of parameters over which the modulated phase occurs is

$$d_B^2 < l_B^2 < (d_B^2 + (\kappa_u/\kappa_c)^2)(1 + (\kappa_u/\kappa_c)^2). \tag{3.13}$$

We note that in the elastic free energy density (Eq. (3.4)) we have not taken into consideration certain symmetry- allowed terms fourth order in $\mathbf{q}$ and second order in fields (*e.g.*, $(\nabla^2\delta c)^2$). Inclusion of such terms broadens the stability range of the modulated phase.

3.3 The modulated phase

To analyse the modulated phase we use the single- wavevector ansatz

$$u(\mathbf{x}) = a\,\cos(p_x x + p_y y + p_z z), \tag{3.14}$$

where a is the modulation amplitude. The δc- field corresponding to this ansatz is given via Eq. (3.8). The average free energy of the modulated phase obtained by using the ansatz Eq. (3.14) and the corresponding δc- field, in the free energy (given via Eq. (3.4), with the K_ϕ- term neglected), and integrating over one spatial period is

$$\langle f_{\rm eff} \rangle = \frac{A^2 B}{4} \, \frac{g(\mathbf{p})}{1 + \kappa_c^2 \, p^2}, \tag{3.15}$$

with the rescaled modulation amplitude $A = a/\xi$. Introducing any additional and independent periodic variation in the decoupled field $\delta\phi$ in the ansatz for the modulated phase increases the average free energy over one period, and is therefore ruled out.

Minimization of the averaged effective free energy (Eq. (3.15)) (neglecting the sixth order term in $g(\mathbf{p})$) with respect to $\mathbf{p}$ yields the square of the wavenumber

$$p^2 \simeq \frac{(l_B/d_B)^2 - 1}{\kappa_u^2 + (l_B/d_B)^2 \, \kappa_c^2}, \tag{3.16}$$

and the direction of the wavevector via

$$\tan 2\theta \simeq \frac{2 \, l_B \, \kappa_c^2}{\kappa_u^2 + (l_B/d_B)^2 \, \kappa_c^2}, \tag{3.17}$$

where $\tan\theta = p_x/p_z$. The modulation wavevector lies in the xz- plane. This is expected, since the L- term couples distortions in the xz- plane alone. Taking K_u and K_c to be of the order of the Frank elastic constants ($\sim 10^{-7}$ dyne), the layer compression modulus $B \sim 10^7 \, \mathrm{dyne\,cm^{-2}}$ [10], and using the fact that the correlation length ξ is of the order of the smectic layer spacing $d \sim 10^{-7}$ cm [1], we get $\kappa_c d_B = \alpha \, d^{-1} \sqrt{K_c/B} \sim 1$ and $\kappa_u \sim 1$. Numerical minimization the full, averaged effective free energy (Eq. (3.15)) (retaining the sixth order term in $g(\mathbf{p})$) with these parameter values gives us the dependence of the components of the dimensionless wavevector on $\mu \equiv (l_B^2/d_B^2 - 1)$ (see Fig. 3.2). For parameter values mentioned in Fig. 3.2, the stability range (Eq. (3.13)) of the modulated phase is $0.1 \lesssim l_B^2 \lesssim 0.25$. The amplitude of modulation is governed by higher order terms in the fields δc- and u- in the free energy, and cannot be obtained within the linear theory considered here.

The condition $L^2 > BD$ suggests that the modulated phase can be expected only in materials which are very soft (in that D is small). The modulated instability is primarily driven by a competition between the elastic constants L, D and B. The instability condition does not directly depend upon the nature (type-I or -II) of SmC. However, for small values of D the penetration depth λ_c is likely to be large. It is therefore quite possible that the modulated phase is favoured

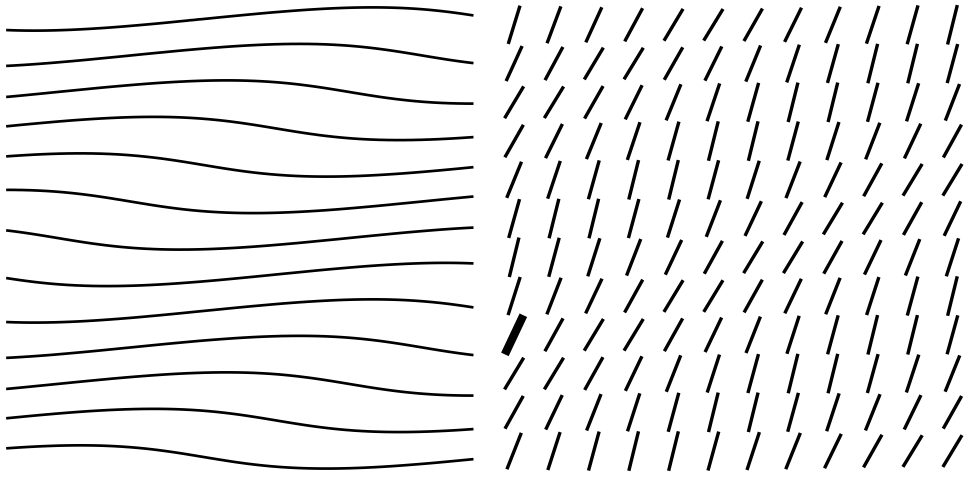

(a) Layer structure. (b) Director field $\mathbf{n}$.

Figure 3.3: Schematic (exaggerated) of the modulated phase. The bold segment in (b) shows director orientation in undistorted SmC. In the experiment discussed (see the text), the polarizer was placed along this direction, and the analyser orthogonal to it. *Although there is no translational order within the layers, line segments are placed periodically to emphasize the stripe structure*.

in type-II materials.

3.4 A previous experimental observation

In what follows, we discuss a previous experiment in which stripe patterns consistent with the proposed structure were observed. We first examine properties of the material used in this experiment. Some dopants are known to enhance the type-II character of mixtures of mesogens. For example, 2-cyano-4-heptylphenyl-4'-pentyl-4-biphenyl carboxylate (7CN5) exhibits the nematic phase with SmC-like (also called skew cybotactic) short-range order over a wide range of temperatures. Adding 7CN5 to a chiral compound exhibiting the SmC* phase induces the TGB$_A$ phase, and at a higher concentration, a second, three-dimensionally modulated TGB phase [35]. Electroclinic measurements clearly show a rapid decrease in the elastic constant D with concentration of 7CN5 [41]. Indeed, freeze- fracture electron microscopic studies on the three-dimensionally modulated phase demonstrate that the mixture has an extreme type-II character, with Ginzburg parameter ~ 100, two orders of magnitude larger than that needed for the type-II label [37].

Interestingly, experimental studies have also been made on mixtures of an achiral compound exhibiting the SmC phase with 7CN5 [7]. When the mixture is taken in a cell with walls treated

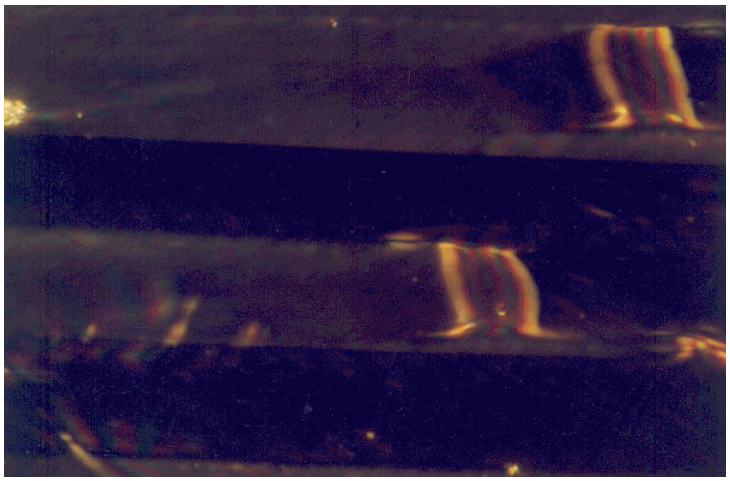

Figure 3.4: The stripe pattern described in [7] and discussed in the text. The orientation of $\mathbf{n}$ differs by $\sim 3^\circ$ between the adjacent domains. The width of the domains is $\sim 40\mu$m. The polarizer was aligned so as to cross out one of the domains (Courtesy: [8]).

for planar alignment of the Frank director $\mathbf{n}$, the transmitted intensity is crossed out in the nematic phase between appropriately placed crossed polarizers. As the sample is slowly cooled across the two-phase region to the SmC phase, it develops a stripe pattern oriented along $\mathbf{n}$ (see Fig. 3.4). The cell has to be reoriented by $\pm 1.5^\circ$ to get a dark field of view in adjacent stripes, which have a width of about 40μm [7, 8]. This observation can be understood if the director pattern of the mixture, which is expected to have a very low value of D, is as shown schematically in Fig. 3.3(b). The wavelength of the observed modulation is $\sim 80\mu$m, and the tilt angle amplitude is $\sim 1.5^\circ$. This would imply that the deviations from a planar layer structure are quite small.

3.5 Some other well known instabilities

Here we discuss some other well known instabilities in layered systems. We compare the mechanism and the structures formed in these cases, to the modulated phase we propose.

3.5.1 The Helfrich instability

The Helfrich instability is well known in smectics. If a uniform stretching deformation is applied to a sample of SmA, of thickness h, undulations are produced with a characteristic wavenumber that depends on the sample thickness.

The rotationally invariant nonlinear free energy density for SmA is [42] $F = \int \mathrm{d}^3x f$ where

$$f = \frac{1}{2}\rho_0 B' \left[(\nabla_z u) - \frac{1}{2}(\nabla_x u)^2 - \frac{1}{2}(\nabla_y u)^2)\right] + K_1 \left(\nabla^2 u\right)^2 \tag{3.18}$$

To see that this free energy is indeed rotationally invariant, consider a SmA sample with the layer normal along z- direction. Under a uniform rotation around the y-axis, the wavevector $\mathbf{q}_0$ describing the smectic density modulation goes to $\mathbf{q}_0 = q_0(\cos\theta\,\mathbf{e}_z - \sin\theta\,\mathbf{e}_x)$. Then (see [1]),

$$\begin{aligned} q_0\, u &= q_0\left[(1-\cos\theta)\, z - \sin\theta\, x\right] \\ \nabla_{\parallel} u &= \nabla_z u = 1 - \cos\theta \\ \nabla_{\perp} u &= \nabla_x u = -\sin\theta. \end{aligned} \tag{3.19}$$

Therefore, the combination $\left[(\nabla_z u) - \frac{1}{2}(\nabla_x u)^2 - \frac{1}{2}(\nabla_y u)^2)\right] = 1 - \cos\theta - \left[(1-\cos\theta)^2 + \sin^2\theta\right] = 0$ is independent of θ.

We assume that the sample is finite, with thickness h in the z- direction and that the xy-plane lies in the middle of the sample ($h = 0$). Putting $u = \gamma z + \delta u(x, z)$, where δu is small and satisfies the boundary conditions $\delta u = 0$ for $z = \pm h$, we get,

$$F = \frac{1}{2}\int \left[\rho_0 B' \left(\nabla_z \delta u\right)^2 - \rho_0 B' \gamma (\nabla_x \delta u)^2 + K_1 (\nabla_x^2 \delta u)\right] \mathrm{d}x\mathrm{d}z. \tag{3.20}$$

Using the ansatz $\delta u = a \times \cos k_z z\, \cos k_x x$, where a is the amplitude of modulation and $k_z = \frac{n\pi}{h}$ for $n = 1, 2, 3...$, we obtain the stability condition

$$\rho_0 B'(k_z^2 - \gamma k_x^2) + K_1\, k_x^4 > 0 \tag{3.21}$$

The critical value of γ for which the above stability condition is violated, and the corresponding value of k_x is given by

$$\gamma_{cr} = \left(\frac{2\pi}{h}\right)\left(\frac{K_1}{\rho_0 B'}\right)^{\frac{1}{2}},\ k_{cr} = \left(\frac{\pi}{h}\right)\left(\frac{K_1}{\rho_0 B'}\right)^{\frac{1}{2}} \tag{3.22}$$

3.5.2 Striped structures in SmC and SmC* materials

Johnson and Saupe [43] found that a material undergoing SmA-SmC transition exhibited a striped pattern upon step-by-step cooling across the transition temperature, with the stripes par-

allel to the c-vector. Upon further cooling, the material developed a rectangular grid pattern. The Johnson-Saupe instability has two orthogonal wavevectors in the plane of the layers and occurs in cells treated such that the smectic layering is parallel to the cell walls. The instability occurs as a result of the reduction in the smectic layer thickness as the director tilt increases. The spacers holding the sample contract less than the smectic layers themselves, which undulate to fill the gap created by the contraction of the layers. This is a *metastable* undulation instability which falls in the class of other well known field-induced instabilities such as the Helfrich instability described above. The modulated phase we propose is an equilibrium structure and has a wave-vector in the $\mathbf{N}_0$-$\mathbf{c}_0$ plane.

Stripe structures have been observed in SmA* materials in samples treated for "bookshelf" alignment, when cooled to the SmC* phase. The samples taken were thin ($\sim 10\mu m$), so that the SmC* helix is suppressed. These stripe structures have been attributed to chiral (and hence polarization terms) in the free energy. Strangi *et al.* [44] have reported the observation of a "horizontal chevron structure", whose origin has been traced to the surface anisotropy of the cell boundaries. The polarization vector prefers to align parallel to the bounding surface, and the formation of domains with parallel and anti-parallel alignment of the polarization vector minimizes the energy. Tang *et al.* [45] have used a Landau-de Gennes free energy involving a chiral term to analyse stripes formed in a similar system:

$$\mathcal{F} = \frac{a}{2}\left|\mathbf{c}\right|^2 + \frac{b}{4}\left|\mathbf{c}\right|^4 + \lambda\left|\mathbf{c}\right|^2 \mathbf{e}_z \cdot (\nabla \times \mathbf{c}) + \frac{K_s}{2}(\nabla \cdot \mathbf{c})^2 + \frac{K_B}{2}(\nabla \times \mathbf{c})^2 \tag{3.23}$$

where $\mathbf{c}$ is the c-vector in the SmC* phase and the SmA*-SmC* transition occurs when the coefficient a goes negative. Chirality is taken into account through the term $\lambda\left|\mathbf{c}\right|^2 \mathbf{e}_z \cdot (\nabla \times \mathbf{c})$ in the free energy. The modulated phase we propose does not require the material to be chiral, and is not a surface effect.

3.5.3 Ripple phases in lipid bilayers

Modulated equilibrium structures (ripple phases) are observed in lamellar lyotropic systems on lowering the temperature across the chain- melting transition [46]. Chen, Lubensky and MacKintosh [47, 48] have proposed a theoretical model, which is based upon a free energy exhibiting a Lifshitz point. In this model, the instability is driven by an elastic coupling between membrane curvature and molecular tilt. They work with the elastic variables $\mathbf{m}$, which is the projection of the molecules on to the plane of the layers, and $h(x, y)$, which is the height of the distorted membrane relative to some Euclidean plane with coordinates (x, y) (so that $\nabla_i \nabla_j h(x, y)$ is the

curvature tensor). The model free energy is composed of two parts: one describing the distortions of $\mathbf{m}$, and the other describing the curvature of the layers. The second part involves a term that couples the layer curvature to the gradients in molecular tilt.

The distortions in $\mathbf{m}$ are described by the elastic free energy density

$$f_m = \frac{1}{2}C_{\parallel}\left(\nabla\cdot\mathbf{m}\right)^2 + \frac{1}{2}C_{\perp}\left(\nabla\times\mathbf{m}\right)^2 + \frac{1}{2}D\left(\nabla^2\mathbf{m}\right)^2 + \frac{1}{2}t\,\mathbf{m}^2 + u\,\mathbf{m}^4, \tag{3.24}$$

and the free energy density for the curvature of the layers is

$$f_c = \frac{1}{2}\kappa\left(\nabla^2 h\right)^2 - \gamma\left(\nabla^2 h\right)^2(\nabla\cdot\mathbf{m}). \tag{3.25}$$

In equilibrium, $h(x,y)$ is given by the Euler-Lagrange equation

$$\left(\nabla^2 h\right)^2 = \frac{\gamma}{\kappa}(\nabla\cdot\mathbf{m}). \tag{3.26}$$

Using this in Eq. (3.25), we obtain the total free energy density in terms of the $\mathbf{m}$- field alone:

$$f_m = \frac{1}{2}C'_{\parallel}\left(\nabla\cdot\mathbf{m}\right)^2 + \frac{1}{2}C_{\perp}\left(\nabla\times\mathbf{m}\right)^2 + \frac{1}{2}D\left(\nabla^2\mathbf{m}\right)^2 + \frac{1}{2}t\,\mathbf{m}^2 + u\,\mathbf{m}^4, \tag{3.27}$$

where $C'_{\parallel} = C_{\parallel} - (\gamma^2/\kappa)$. If $C'_{\parallel} > 0$, the equilibrium phases are spatially uniform. If $C'_{\parallel} < 0$, the the equilibrium phases are spatially modulated with a characteristic wavenumber $q_0 = \sqrt{C'_{\parallel}/2D}$.

Chen, Lubensky and MacKintosh work with a single wavenumber ansatz and predict modulated phases with four different symmetries. They call this the $P^{(1)}_{\beta'}$, $P^{(2)}_{\beta'}$, $P^{(3)}_{\beta'}$ and the square lattice vortex phase. The first three are modulated in one direction, whereas the square lattice vortex phase has two-dimensional modulation and exhibits a vortex-antivortex square lattice in the $\mathbf{m}$- field.

Asymmetric ripple phases have been studied and a theoretical model has been proposed [49]. This model includes nonlinear terms in addition to the ones used above (see Eqs. (3.24) and (3.25)) to describe the observed asymmetry in the bilayer thickness of the two arms of the ripple. The additional nonlinear terms introduced are

$$f_{nl} = \frac{\beta}{4}(\nabla\cdot\mathbf{m})^4 + \frac{\xi}{2}\left[(\mathbf{m}\cdot\nabla)\mathbf{m}\right]^2 + \frac{\zeta}{2}\left[(\mathbf{m}\times\nabla)\mathbf{m}\right]^2, \tag{3.28}$$

where the first term is required for stability, and the second and third terms describe gradients of $\mathbf{m}$ along $\mathbf{m}$ and perpendicular to $\mathbf{m}$ respectively. The last two terms account for the symmetry-allowed anisotropy in the elastic field $\mathbf{m}$. In this model, the square lattice vortex phase is not an

stable equilibrium phase.

The modulated phase we predict differs from the ripple phase in both the mechanism and the resulting structure.

Chapter 4

SmC dislocation energetics and the structure of the TGB_C phase

4.1 Introduction

In this chapter, we derive the equations for the elastic free energy of an arbitrary dislocation density in a SmC material. Our discussion follows that of [18]. The crucial difference in our calculations is the inclusion of the L term in the free energy, which couples layer compression with changes in the director tilt angle. We find that the inclusion of this term in the free energy gives rise to qualitatively new results. The show that the *lowest energy dislocation line is a mixed dislocation line*. This is markedly different from that for SmA, where the screw dislocation line is the lowest energy dislocation line. We calculate the interaction energies between dislocation lines and between low angle grain boundaries (modelled as arrays of dislocation lines).We find that the lowest energy grain boundary is made of the lowest energy dislocation lines, which are mixed dislocation lines.

Though the TGB_C structure originally predicted by Renn and Lubensky [17] involved screw dislocations, subsequent X-ray studies [27] have indicated the presence of a TGB_C phase made up of mixed dislocation lines (the Bordeaux TGB_C structure). Motivated by our result that the lowest energy dislocation line in the SmC phase is a mixed dislocation line, we study the energetics of the TGB_C phase in order to see if the presence of the L term stabilizes the Bordeaux structure. Our analysis is close to the lower critical field, where the SmC phase becomes unstable to the TGB_C phase. Here, the angle of rotation between the adjacent grain boundaries is small and we can treat the grain boundaries as arrays of dislocation lines. The analysis we do is based on a linear theory [18] and the dislocation complexion is similar to that discussed in Chapter

2. We study the structure of the TGB$_C$ phase close to the lower critical field and find that even though *at* the lower critical field, the minimum energy dislocation line is a mixed dislocation line, minimizing the Gibbs free energy (including interactions) suggests that a TGB$_C$ structure made of screw dislocation lines is preferred. Further work on this is in progress.

4.2 Dislocations in Smectic-C

As shown in Chapter 3, the elastic free energy for SmC can be written in terms of the layer displacement field $u(\mathbf{x})$, and the change in the magnitude of the $\mathbf{c}$-vector, $\delta c(\mathbf{x})$. In the presence of dislocations, the the gradient of the u- field can be written as the sum of an analytic and a singular part as

$$\nabla u(\mathbf{x}) = \nabla u^{(a)}(\mathbf{x}) + \mathbf{v}(\mathbf{x}), \tag{4.1}$$

with

$$\nabla \times \mathbf{v}(\mathbf{x}) = \mathbf{b}(\mathbf{x}), \tag{4.2}$$

where

$$\mathbf{b}(\mathbf{x}) = \mathbf{e}_z \sum_\mu k_\mu \, d \int \mathrm{d}s \, \delta(\mathbf{x} - \mathbf{R}_\mu(s)) \tag{4.3}$$

is the dislocation line density and d is the layer spacing. Here $\mathbf{R}_\mu(s)$ is the position of dislocation μ with strength k_μ as a function of arclength s. $\mathbf{v}(\mathbf{x})$ can always be chosen to have zero divergence (see section 2.2.2). Therefore, in the Fourier domain, we can write

$$\mathbf{v}(\mathbf{q}) = i \frac{\mathbf{q} \times \mathbf{b}(\mathbf{q})}{q^2}. \tag{4.4}$$

As discussed in Chapter 3, the elastic free energy for distortions from the SmC ground state is $F = \int \mathrm{d}^3x \, f$, where f is given by

$$f = \frac{B}{2}(\partial_z u)^2 + \frac{D}{2}(\delta c + \alpha \, \partial_x u)^2 - L(\delta c + \alpha \, \partial_x u)(\partial_z u) + \frac{K_u}{2}(\nabla^2 u)^2 + \frac{K_c}{2}(\nabla \delta c)^2 + \frac{K_\phi}{2}(\nabla \phi)^2. \tag{4.5}$$

This expression for the free energy is quadratic in the the gradients of the u- field and the δc-field. In the presence of dislocations, the gradients of the u- field can be expressed solely in terms of the dislocation source $\mathbf{b}(\mathbf{x})$ using Eqs. (4.1) and (4.2), and we can write the elastic free energy uniquely in terms of the dislocation source. To recast the above equation in terms of the dislocation density $\mathbf{b}(\mathbf{x})$, it is convenient to work in the Fourier domain. We proceed as follows.

Putting Eq. (4.1) in Eq. (4.5), and going to the Fourier domain, we can write

$$F = \frac{1}{2}\int \frac{\mathrm{d}^3 q}{(2\pi)^3}\left[{\Phi^\dagger}_a G^{-1}_{ab}\Phi_b + {\lambda_a}^\dagger\,\Phi_a + {\Phi_a}^\dagger\,\lambda_a + B{v_z}^2 + \alpha^2 D{v_x}^2 - 2\alpha L v_x v_z\right], \tag{4.6}$$

where $\Phi_1 = u^{(a)}(\mathbf{q})$ and $\Phi_2 = \delta c(\mathbf{q})$,

$$G^{-1}(\mathbf{q}) = \begin{pmatrix} Bq_z^2 + \alpha^2 D q_x^2 - 2\alpha L q_x q_z + K_u q^4 & i(Lq_z - \alpha D q_x) \\ -i(Lq_z - \alpha D q_x) & D + K_c q^2 \end{pmatrix}, \tag{4.7}$$

and

$$\lambda(\mathbf{q}) = \begin{pmatrix} i\left[\alpha L\, q_x v_z(\mathbf{q}) + \alpha L\, q_z v_x(\mathbf{q}) - \alpha^2 D\, q_x v_x(\mathbf{q}) - B\, q_z v_z(\mathbf{q})\right] \\ \alpha D\, v_x(\mathbf{q}) - L\, v_z(\mathbf{q}) \end{pmatrix}. \tag{4.8}$$

Equation (4.6) gives Euler Lagrange equation for the fields $u(\mathbf{q})$ and $\delta c(\mathbf{q})$ as

$${G^{-1}}_{ab}(\mathbf{q})\Phi_b = \lambda_a(\mathbf{q}), \tag{4.9}$$

whose solution is $\Phi_a = G_{ab}(\mathbf{q})\lambda_b(\mathbf{q})$. This gives us an expression for the analytic fields $u(\mathbf{q})$ and $\delta c(\mathbf{q})$ in terms of $v(\mathbf{q})$, the singular part of the gradient of the u- field (in Fourier space). Substituting this expression for Φ in Eq. (4.6) for the free energy, we obtain the free energy in the presence of dislocations:

$$\begin{aligned} F = \frac{1}{2}\int \frac{\mathrm{d}^3 q}{(2\pi)^3}\,\big[&-\lambda_a^\dagger(\mathbf{q})G_{ab}(\mathbf{q})\lambda_b(\mathbf{q}) + B\,|v_z(\mathbf{q})|^2 \\ &+\alpha^2 D\,|v_x(\mathbf{q})|^2 - \alpha L\,(v_x(\mathbf{q})v_z(-\mathbf{q}) + v_x(-\mathbf{q})v_z(\mathbf{q}))\big]\,. \end{aligned}$$

For simplicity, we set $\alpha^2 D = B$ in the following analysis. Then, using Eq. (4.4), we can express the free energy in terms of the dislocation source $\mathbf{b}(\mathbf{q})$ as

$$F = \frac{1}{2}\int \frac{\mathrm{d}^3 q}{(2\pi)^3}\mathbf{b}^i(\mathbf{q})U_{ij}(\mathbf{q})\mathbf{b}^j(-\mathbf{q}), \tag{4.10}$$

where

$$U_{ij}(\mathbf{q}) = \frac{\tilde{U}_{ij}(\mathbf{q})}{q^2\Delta(\mathbf{q})}, \tag{4.11}$$

$$\Delta(\mathbf{q}) = (\alpha^{-2}B + K_c q^2)(B(q_x^2 + q_z^2) + K_u q^4 - 2\alpha L q_x q_z) - (Lq_z - \alpha^{-1}Bq_x)^2, \tag{4.12}$$

and $\tilde{U}_{ij}(\mathbf{q})$ are given by

$$\begin{aligned}
\tilde{U}_{xx}(\mathbf{q}) &= BK_cK_uq^4q_y^2 + B_LK_cq_x^2q_y^2 + \alpha^{-2}B_LK_uq^2q_y^2, \\
\tilde{U}_{yy}(\mathbf{q}) &= BK_cK_uq^4(q_x^2+q_z^2) + B_LK_c(q_x^4+q_z^4) + \alpha^{-2}B_LK_uq^2q_x^2 \\
&\quad + 2B_LK_cq_x^2q_z^2 + 2\alpha LK_cK_uq^4q_xq_z, \\
\tilde{U}_{zz}(\mathbf{q}) &= BK_cK_uq^4q_y^2 + B_LK_cq_z^2q_y^2, \\
\tilde{U}_{xy}(\mathbf{q}) &= -BK_cK_uq^4q_xq_y - B_LK_cq_x^3q_y - \alpha^{-2}B_LK_uq^2q_xq_y \\
&\quad - B_LK_cq_xq_yq_z^2 - \alpha LK_cK_uq^4q_yq_z, \\
\tilde{U}_{yz}(\mathbf{q}) &= -B_LK_cq_x^2q_yq_z - \alpha LK_cK_uq^4q_xq_y - B_LK_cq_yq_z^3 \\
&\quad - BK_cK_uq^4q_yq_z, \\
\tilde{U}_{zx}(\mathbf{q}) &= B_LK_cq_xq_y^2q_z + \alpha LK_cK_uq^4q_y^2,
\end{aligned} \tag{4.13}$$

where $B_L = (B^2 - \alpha^2L^2)$.

4.2.1 Energy per unit length of a single dislocation line

A single straight dislocation line with its core along a unit vector $\mathbf{e}$, with a Burgers vector of magnitude d is described by

$$\mathbf{b}(\mathbf{x}) = \mathbf{e}\, d\, \delta_e^{(2)}(\mathbf{x}_\perp), \tag{4.14}$$

where $\delta_e^{(2)}(\mathbf{x}_\perp)$ is the two-dimensional Dirac delta function in a plane perpendicular to $\mathbf{e}$. In Fourier space, we can write

$$\mathbf{b}(\mathbf{q}) = \mathbf{e}\, 2\pi d\, \delta(\mathbf{q}\cdot\mathbf{e}) = \mathbf{e}\, d\, L\, \delta_{\mathbf{q}\cdot\mathbf{e},0}. \tag{4.15}$$

The energy per unit length of this dislocation line is then (from Eq. (4.10))

$$\frac{F}{L} = \frac{1}{2}\, d^2 \int_0^{\xi^{-1}} \frac{\mathrm{d}^2 q_e}{(2\pi)^2}\, U(\mathbf{e}), \tag{4.16}$$

where $\mathbf{q}_e = \mathbf{q} - (\mathbf{q}\cdot\mathbf{e})\mathbf{e}$ lies in the plane perpendicular to $\mathbf{e}$ and

$$U(\mathbf{e}) = e^i\, U_{ij}(\mathbf{q}_e)\, e^j. \tag{4.17}$$

In Eq. (4.16), the upper limit of the integral, ξ^{-1}, is the inverse of the smectic correlation length. The upper limit is essential in this expression because elasticity theory for the SmC phase is not

valid at extremely short distances ($\sim \xi$) where the smectic order breaks down. The diameter of the dislocation core is also of the order of ξ.

Dislocation line in the xz- plane

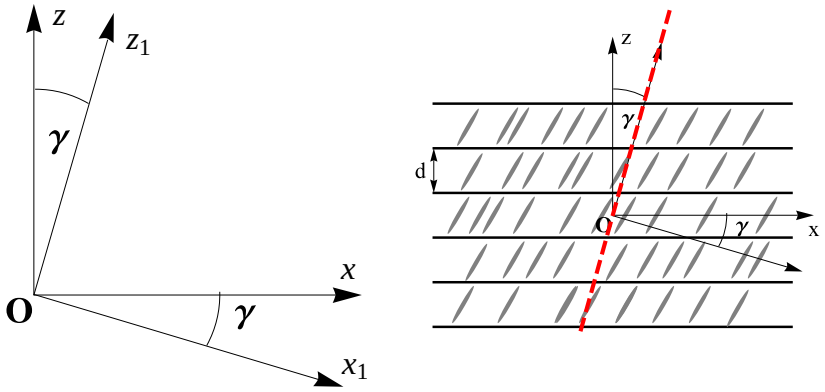

(a) The coordinate system

(b) Schematic of SmC, with orientation of the the mixed dislocation line shown in red.

Figure 4.1: The coordinate system. The layer normal $\mathbf{N}_0$ points along $\mathbf{e}_z$. The $\mathbf{x}_1 = (x_1, y_1, z_1)$ coordinate system is rotated with respect to the $\mathbf{x} = (x, y, z)$ coordinate system by an angle γ about the $y-$ axis. The dislocation line lies in the $xz-$ plane and makes an angle γ with $\mathbf{e}_z$, *i.e.*, it points along $\mathbf{e}_{z_1}$

For a dislocation line in the xz- plane, $\mathbf{e} = \sin\gamma\,\mathbf{e}_x + \cos\gamma\,\mathbf{e}_z$ as shown in the Fig. 4.1, where $\mathbf{e}_z$ is along the layer normal. For this dislocation, it is convenient to go to the $\mathbf{x}_1 = (x_1, y_1, z_1)$ coordinate system, which is related to the $\mathbf{x} = (x, y, z)$ coordinate system through a rotation by an angle γ around the y- axis.

$$\begin{pmatrix} x_1 \\ y_1 \\ z_1 \end{pmatrix} = \begin{pmatrix} \cos\gamma & 0 & \sin\gamma \\ 0 & 1 & 0 \\ -\sin\gamma & 0 & \cos\gamma \end{pmatrix} \begin{pmatrix} x \\ y \\ z \end{pmatrix}, \tag{4.18}$$

Expressed in the $\mathbf{x}_1$ coordinate system, $\mathbf{b}(\mathbf{x}_1) = \mathbf{e}_{z_1}\, d\, \delta(x_1)\delta(y_1)$ (see Fig. 4.1) and

$$\begin{aligned} \mathbf{b}(\mathbf{q}_1) &= \mathbf{e}_{z_1}\, d \int \mathrm{d}^3\mathbf{x}_1\, \delta(x_1)\delta(y_1) e^{i\mathbf{q}_1\cdot\mathbf{x}_1} \\ &= 2\pi d\, \mathbf{e}_{z_1}\, \delta(q_3), \end{aligned} \tag{4.19}$$

where the rotated wave-vector $\mathbf{q}_1 = (q_1, q_2, q_3)$ is given by

$$\begin{pmatrix} q_1 \\ q_2 \\ q_3 \end{pmatrix} = \begin{pmatrix} \cos\gamma & 0 & \sin\gamma \\ 0 & 1 & 0 \\ -\sin\gamma & 0 & \cos\gamma \end{pmatrix} \begin{pmatrix} q_x \\ q_y \\ q_z \end{pmatrix}. \tag{4.20}$$

Then, $\mathbf{q}_e = (q_1, q_2)$ and Eq. (4.16) can be written as

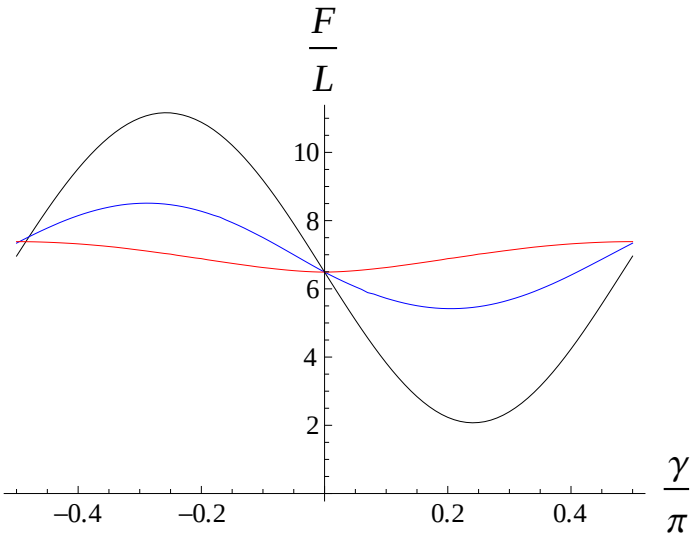

Figure 4.2: The elastic energy per unit length F/L (measured in units of $Bd^2/4\pi^2$) of a single dislocation line in the xz- plane, versus the angle γ it makes with the layer normal. The plots are shown for $\delta = -0.75$ (black), $\delta = -0.25$ (blue) and $\delta = 0$ (red). For these plots we have chosen $\beta = 3$ and $\xi^{-1}\tilde{\lambda}_c = 10$. The minimum energy dislocation line for nonzero δ is a mixed dislocation line.

$$\frac{F}{L} = \frac{1}{2}\, d^2 \int_0^{\xi^{-1}} \frac{\mathrm{d}^2 q_e}{(2\pi)^2} \left[\frac{\cos^2\gamma\, \tilde{U}_{zz}(\mathbf{q}_e) + 2\cos\gamma\sin\gamma\, \tilde{U}_{xz}(\mathbf{q}_e) + \sin^2\gamma\, \tilde{U}_{xx}(\mathbf{q}_e)}{q^2 \Delta(\mathbf{q}_e)} \right]. \tag{4.21}$$

With the substitutions $\lambda_u^2 = K_u/B$, $\lambda_c^2 = K_c/B$, $\tilde{\lambda}_c^2 = \alpha^2\lambda_c^2$, $\delta = \alpha L/B$ and $\mathbf{q}_e = (q1, q2) = (q\cos\theta, q\sin\theta)$, Eq. (4.21) can be written as

$$\frac{F}{L} = \frac{1}{2}\,\frac{Bb^2}{4\pi^2} \int_0^{\xi^{-1}} \mathrm{d}q \int_0^{2\pi} \mathrm{d}\theta\, \frac{\left[\tilde{\lambda}_c^2 q^2\,(1 + 2\delta\,\sin\gamma\,\cos\gamma) + (1-\delta^2)\sin^2\gamma\right]\sin^2\theta}{\lambda_u^2 q^2(1+\tilde{\lambda}_c^2 q^2) + \left[\tilde{\lambda}_c^2 q^2\,(1 + 2\delta\,\sin\gamma\,\cos\gamma) + (1-\delta^2)\sin^2\gamma\right]\cos^2\theta}. \tag{4.22}$$

In terms of $p = \tilde{\lambda}_c\, q$, using $\beta = \tilde{\lambda}_c/\lambda_u$, and choosing $\xi^{-1}\tilde{\lambda}_c = 10$ we have,

$$\frac{F}{L} = \frac{1}{2}\,\frac{Bb^2}{4\pi^2}\int_0^{10} \mathrm{d}p \int_0^{2\pi} \mathrm{d}\theta \frac{\left[p^2\,(1+2\delta\,\sin\gamma\,\cos\gamma) + (1-\delta^2)\sin^2\gamma\right]\sin^2\theta}{\beta^{-2}p^2(1+p^2) + \left[p^2\,(1+2\delta\,\sin\gamma\,\cos\gamma) + (1-\delta^2)\sin^2\gamma\right]\cos^2\theta}. \tag{4.23}$$

The above integral was numerically evaluated. From Fig. 4.2, we can immediately see that the minimum energy dislocation line is not a screw dislocation line (as in SmA), but a mixed dislocation line. Previous calculations [18] neglecting the L- term in the free energy density give the result that the minimum energy dislocation line in the SmC phase is a screw dislocation line. One can understand our result from the observation that the L- term couples gradients of u along the x- and z- directions, which implies that the system may favour a deformation involving both $\nabla_z u$ and $\nabla_x u$ to one that involves $\nabla_x u$ or $\nabla_z u$ alone . Indeed, tracing back each term in Eq. (4.23) to the free energy in Eq. (4.5), we find that it is the term $-L(\nabla_z u)(\nabla_x u)$ which gives rise to this result.

Dislocation line in the yz- plane

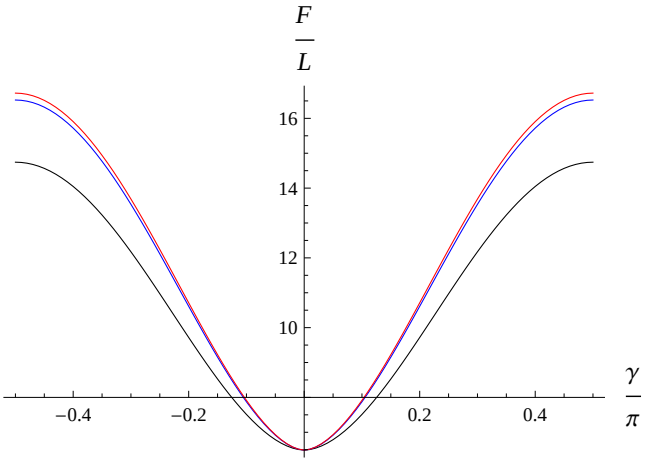

Figure 4.3: The elastic energy per unit length F/L (measured in units of $Bd^2/4\pi^2$) of a single dislocation line in the yz- plane, versus the angle γ it makes with the layer normal. The plots are shown for $\delta = -0.75$ (black), $\delta = -0.25$ (blue) and $\delta = 0$ (red). For these plots we have chosen $\beta = 3$ and $\xi^{-1}\tilde{\lambda}_c = 10$. The minimum energy dislocation line is a screw dislocation line.

For a dislocation line in the yz- plane, $\mathbf{e}$ lies in the yz- plane, and makes an angle γ with$\mathbf{e}_z$. The $\mathbf{x}_1 = (x_1, y_1, z_1)$ coordinate system is related to the $\mathbf{x} = (x, y, z)$ coordinate system through a rotation by an angle γ around the x- axis. The rest of the calculation is similar to that for the

dislocation line in the xz- plane. Figure 4.3 shows the results. The screw dislocation line has a lower energy as compared to a mixed dislocation line in the yz- plane.

4.2.2 Interaction Potential Energy

Dislocation lines in the xz- plane

Consider two parallel dislocation lines, tilted by an angle γ in the xz- plane (see Fig. 4.1). One dislocation line passes through the origin of the (x_1, y_1, z_1) coordinate system and extends along z_1, and the other passes through the point $(0, \bar{y})$ and is parallel to the first one.

These dislocation lines can be described by $\mathbf{b}_1(\mathbf{x}_1) = \mathbf{e}_{z_1}\, d\, \delta(x_1)\delta(y_1)$ and $\mathbf{b}_2(\mathbf{x}_1) = \mathbf{e}_{z_1}\, d\, \delta(x_1)\delta(y_1 - \bar{y})$ respectively. In Fourier space,

$$\begin{aligned} \mathbf{b}_1(\mathbf{q}_1) &= \mathbf{e}_{z_1}\, d \int \mathrm{d}^3\mathbf{x}_1 \delta(x_1)\delta(y_1) e^{i\mathbf{q}_1\cdot\mathbf{x}_1} \\ &= 2\pi d\, \mathbf{e}_{z_1}\, \delta(q_3), \end{aligned} \tag{4.24}$$

and

$$\begin{aligned} \mathbf{b}_2(\mathbf{q}_1) &= \mathbf{e}_{z_1}\, d \int \mathrm{d}^3\mathbf{x}_1 \delta(x_1)\delta(y_1 - \bar{y}) e^{i\mathbf{q}_1\cdot\mathbf{x}_1} \\ &= 2\pi d\, \mathbf{e}_{z_1}\, \delta(q_3) e^{iq_2\bar{y}}. \end{aligned} \tag{4.25}$$

The interaction potential energy between these two parallel dislocation lines is given by Eq. (4.10)

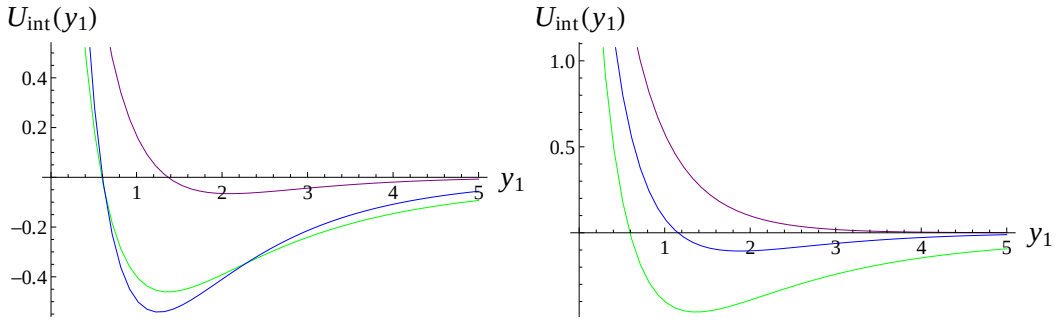

(a) $\delta = 0.75$ (b) $\delta = 0$

Figure 4.4: The interaction potential energy per unit length $U_{\text{int}}(y_1)$ (measured in units of $Bd^2/4\pi^2$) between parallel dislocation lines in the xz- plane, versus the separation (measured in units of $\tilde{\lambda}_c$) between them along the y_1-axiz. The curves are plotted with $\beta = 3$, for $\gamma = 0$ (green), $\gamma = \pi/5$ (blue) and $\gamma = \pi/2$ (purple).

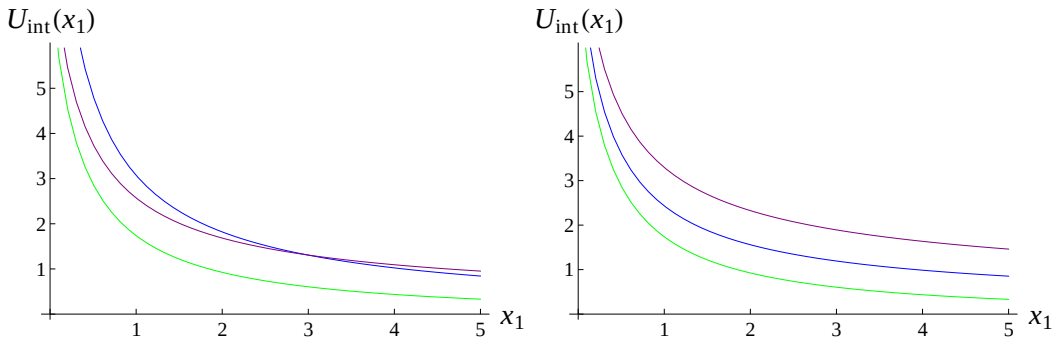

(a) $\delta = 0.75$ (b) $\delta = 0$

Figure 4.5: The interaction potential energy per unit length $U_{\rm int}(x_1)$ (measured in units of $Bd^2/4\pi^2$) between two parallel dislocation lines in the xz- plane, versus the separation (measured in units of $\tilde{\lambda}_c$) between them along the x_1-axis. The curves are plotted for $\gamma = 0$ (green), $\gamma = \pi/5$ (blue) and $\gamma = \pi/2$ (purple). Here, $\beta = 3$.

and can be written as

$$U_{\rm int}(\bar{y}) = d^2 \int_{-\infty}^{\infty} \frac{\mathrm{d}^2 q_e}{(2\pi)^2} U(\mathbf{e}) e^{i\, q_2 \bar{y}}, \tag{4.26}$$

where $\mathbf{q}_e = (q_1, q_2)$. Using $\lambda_u^2 = K_u/B$, $\lambda_c^2 = K_c/B$, $\tilde{\lambda}_c^2 = \alpha^2 \lambda_c^2$, $\delta = \alpha L/B$ (as defined before), the rescaled dimensionless wavenumber $p = \tilde{\lambda}_c q$ and $\beta = \tilde{\lambda}_c/\lambda_u$, we get

$$U_{\rm int}(\bar{Y}) = \frac{Bd^2}{4\pi^2} \int_{-\infty}^{\infty} \mathrm{d}p_1 \mathrm{d}p_2\, \mathcal{U}(p_1, p_2)\, e^{i\, p_2 \bar{Y}}, \tag{4.27}$$

where $\bar{Y} = \bar{y}/\tilde{\lambda}_c$, $\mathcal{U}(p_1, p_2) = \mathcal{N}(p_1, p_2)/\mathcal{D}(p_1, p_2)$ and the polynomials $\mathcal{N}(p_1, p_2)$ and $\mathcal{D}(p_1, p_2)$ are given by

$$\mathcal{N}(p_1, p_2) = (1 + 2\delta\, \sin\gamma \cos\gamma) p_2^4 + ((1 - \delta^2) \sin^2\gamma + p_1^2 (1 + 2\delta\, \sin\gamma \cos\gamma)) p_2^2, \tag{4.28}$$

$$\begin{aligned} \mathcal{D}(p_1, p_2) &= p_2^6 + \left(1 + 3p_1^2\right) p_2^4 + \left(3p_1^4 + p_1^2 \left(2 + \beta^2 \left(1 + 2\delta\, \sin\gamma \cos\gamma\right)\right)\right) p_2^2 \\ &+ p_1^6 + \left(1 + \beta^2 \left(1 + 2\delta\, \sin\gamma \cos\gamma\right)\right) p_1^4 + \left(\left(1 - \delta^2\right) \beta^2 \sin^2\gamma\right) p_1^2. \end{aligned} \tag{4.29}$$

A plot of numerically evaluated $U_{\rm int}(\bar{Y})$ vs. $\bar{Y}$ is shown in Fig. 4.4. We can see that the the interaction along the y- direction is not purely repulsive (as in SmA). This interaction potential has a minimum at $y \sim \tilde{\lambda}_c$, is attractive over large distances ($y >> \tilde{\lambda}_c$) and repulsive over short distances ($y << \tilde{\lambda}_c$).

Similarly, the interaction potential energy between two parallel dislocations in the xz- plane, separated by a distance $\bar{x}_1$ along the x_1- axis (see Fig. 4.1) can be written as

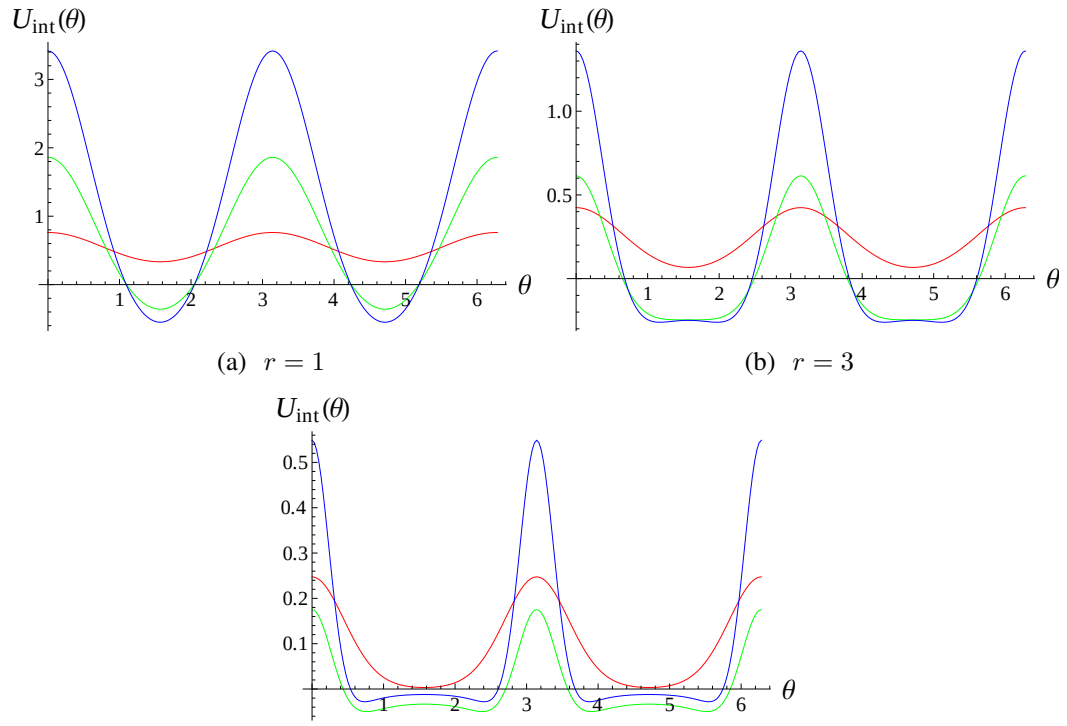

Figure 4.6: The interaction potential energy per unit length $U_{\rm int}(\theta)$ (measured in units of $Bd^2/4\pi^2$) between two parallel dislocation lines in the xz- plane for separations r (measured in units of $\tilde{\lambda}_c$) between them. The curves have been plotted for $\gamma = -\pi/10$ (red), $\gamma = 0$ (green) and $\gamma = \pi/10$ (blue). Here, $\beta = 3$ and $\delta = 9/10$.

$$U_{\rm int}(\bar{X}) = \frac{Bd^2}{4\pi^2}\int_{-\infty}^{\infty} {\rm d}p_1 {\rm d}p_2\, \mathcal{U}(p_1, p_2)\, e^{i\,p_1 \bar{X}}, \tag{4.30}$$

where $\bar{X} = \bar{x}_1/\tilde{\lambda}_c$. A plot of numerically evaluated $U_{\rm int}(\bar{X})$ vs. X is shown in Fig. 4.5. The interaction potential between dislocation lines separated along the x_1- direction is repulsive, as in a SmA material. The anisotropy in the interaction potentials is shown in Fig. 4.6, which is a plot of the interaction potential energy between two parallel dislocation lines along z_1- direction (see Fig. 4.1), as a function of the polar angle θ in the x_1y_1- plane. Here, the distance r between the dislocation lines is kept constant. The difference in the interaction energies along the x_1- and y_1- directions is clearly visible. We can see from the graphs that for small separations mixed

dislocation lines have a lower energy of interaction along $\theta = \pi/2$ and $\theta = 3\pi/2$ (Fig. 4.6(a)), but as for large separations, the screw dislocation has the lowest energy of interaction for all θ (Fig. 4.6(c)).

Dislocation lines in the yz- plane

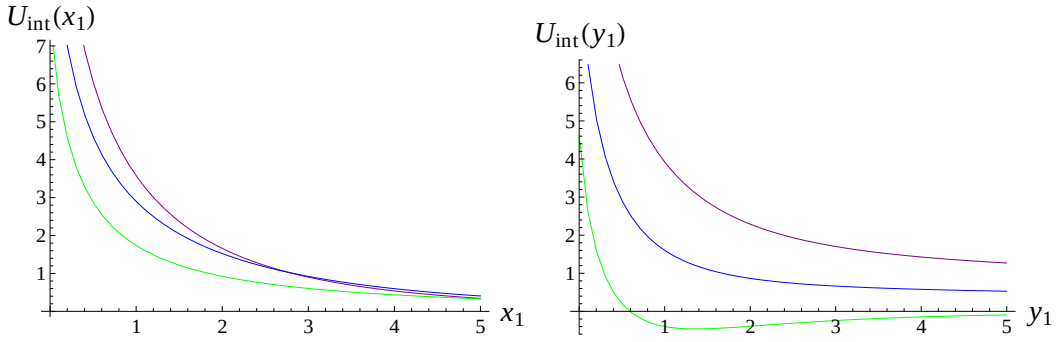

(a) (b)

Figure 4.7: The interaction potential energy per unit length U_{int} (measured in units of $Bd^2/4\pi^2$) between two parallel dislocation lines in the yz- plane, versus the separation (measured in units of $\tilde{\lambda}_c$) between them, along the $(a)\, x_1$-axis, and, $(b)\, y_1$- axis. The curves are plotted for $\gamma = 0$ (green), $\gamma = \pi/5$ (blue) and $\gamma = \pi/2$ (purple). Here, $\beta = 3$ and $\delta = 0.75$.

Consider two parallel dislocation lines, tilted by an angle γ in the yz- plane. The (x_1, y_1, z_1) coordinate system is rotated through an angle γ about $\mathbf{e}_x$. The calculation is similar to that described above for dislocation lines in the xz- plane. The results are shown in Fig. 4.7. Screw dislocation lines have the lowest interaction energy.

4.2.3 Energy per unit area of an array of dislocation lines

Motivated by the results for the elastic energy per unit length and the interaction energy of dislocation lines tilted in the xz- plane, we explore the energetics of a grain boundary made of such dislocation lines. A grain boundary can be modelled as an infinite array of parallel dislocation lines. The energy of an infinite array of dislocation lines, with the plane of the grain boundary being the $y_1 z_1$- plane and the dislocation lines themselves oriented along z_1, can be calculated using Eq. (4.10) if

$$\mathbf{b}_1(\mathbf{x}) = \mathbf{e}_{z1}\, d\, \delta(x_1) \sum_{n=-\infty}^{\infty} \delta(y_1 - n l_d), \tag{4.31}$$

and

$$\mathbf{b}_2(\mathbf{x}) = \mathbf{e}_{z1}\, d\, \delta(x_1) \sum_{m=-\infty}^{\infty} \delta(y_1 - m l_d), \tag{4.32}$$

where l_d is the spacing between the dislocation lines and $\mathbf{e}$ is the unit vector along the direction of the core of the dislocation line. For a finite array with N dislocations lines, the above summations will be from 1 to N. For an array, the total energy can be written of the sum of *(i)* elastic energy of each dislocation line in the array, and, *(ii)* the energy of interaction between each pair of dislocation line.

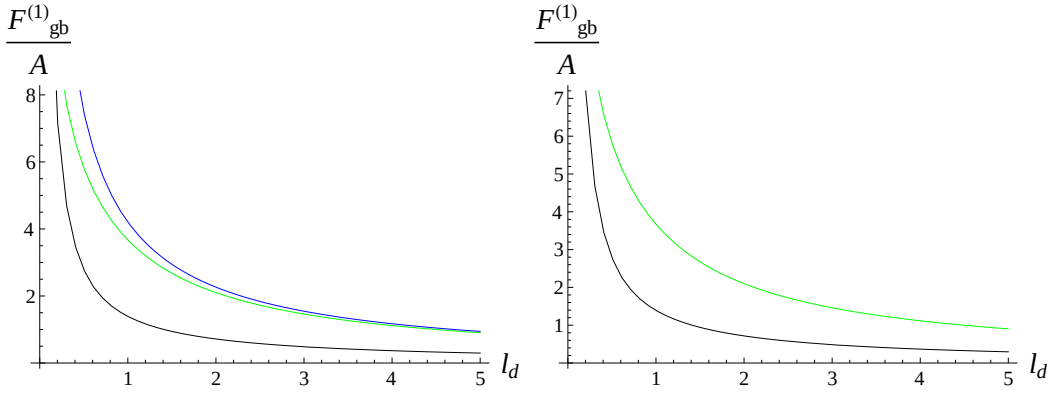

Figure 4.8: The energy per unit area of a grain boundary in the yz_1- plane, $F^{(1)}_{\rm gb}/A$ (measured in units of $Bd^2/4\pi^2\tilde{\lambda}_c$), as a function of the separation l_d (measured in units of $\tilde{\lambda}_c$) between the dislocation lines that make up the grain boundary. Each dislocation line is oriented along $\mathbf{e}_{z_1}$. The curves are plotted for $\gamma = -\pi/2$ (blue), $\gamma = 0$ (green) and $\gamma = 6\pi/25 =$ angle of the minimum energy dislocation line (black), for $N = 50$, $\delta = -3/4$ and $\beta = 3$, with $\xi^{-1}\tilde{\lambda}_c = 10$. Figure (b) clearly shows that *the minimum energy grain boundary is made of the minimum energy dislocation lines.*

The energy per unit area for a finite array is given by

$$\frac{F^{(1)}_{\rm gb}}{A} = F_{\rm int} + \frac{N}{(N-1)L_d\tilde{\lambda}_c}\frac{F^{(1)}_{el}}{L}, \tag{4.33}$$

where

$$F_{\rm int} = \frac{Bd^2}{4\pi^2\,\tilde{\lambda}_c}\frac{\sum_{n>m}^{N}\sum_{m=1}^{N}\int_{-\infty}^{\infty}{\rm d}p_1{\rm d}p_2\,\mathcal{U}(p_1,p_2)e^{i\,p_2(n-m)L_d}}{(N-1)L_d} \tag{4.34}$$

is the interaction potential energy per unit area for this array and $F^{(1)}_{el}/L$ is the self energy per

unit length of a single dislocation line given in Eq. (4.23). Here, $p = \tilde{\lambda}_c q$ and $L_d = l_d/\tilde{\lambda}_c$.

The curves in Fig. 4.8 are monotonically decreasing. This is expected, since the ground state (lowest energy state) of the system is the SmC phase without any dislocations. As l_d increases, the dislocation lines in the array become more and more sparse, and the number of dislocation line in a given area decreases, *ie.*, the system approaches the dislocation-free SmC configuration. *It is found that $F_{\rm gb}^{(1)}/A$ is the lowest for a grain boundary made of the lowest energy dislocation line.*

4.3 The TGB$_C$ phase

The Gibbs free energy per unit volume (see Section 2.6) in the TGB$_C$ phase, in the presence of a chiral field h is obtained by subtracting the chiral energy per unit volume from the energy per unit volume of a lattice of dislocation lines.

$$\frac{G_{\rm tgb}}{V} = \frac{F_{\rm lattice}}{V} - \frac{hd}{l_b l_d}. \tag{4.35}$$

4.3.1 Energy per unit volume of a lattice of dislocation lines

The energy per unit volume for an infinite rectangular lattice (lattice vectors along the x_1- and y_1- directions) of parallel dislocation lines (each dislocation line oriented along z_1-)is given by Eq. (4.10), with the dislocation source given by

$$\mathbf{b}(\mathbf{x}) = \mathbf{e}\, d \sum_{k=-\infty}^{\infty} \delta(x_1 - k l_b) \sum_{n=-\infty}^{\infty} \delta(y_1 - n l_d), \tag{4.36}$$

where l_d is the spacing between the dislocation lines in the y_1- direction and l_b is the spacing between the dislocation lines in the x_1- direction. $\mathbf{e}$ is the unit vector in the direction of the core of the dislocation lines.

For a finite $K \times N$ lattice, the total energy per unit volume is given by

$$\frac{F_{\rm lattice}}{V} = \frac{1}{2}\frac{Bd^2}{4\pi^2\,\tilde{\lambda}_c^2} \frac{\sum_{k=1}^{K}\sum_{l=1}^{K}\sum_{n=1}^{N}\sum_{m=1}^{N} \int_{-\infty}^{\infty} \mathrm{d}p_1 \mathrm{d}p_2\, \mathcal{U}(p_1,p_2)\, e^{i\,p_1\,(k-l)L_b} e^{i\,p_2\,(n-m)L_d}}{(K-1)(N-1)L_b L_d}, \tag{4.37}$$

where $L_b = l_b/\tilde{\lambda}_c$ and $L_d = l_d/\tilde{\lambda}_c$. The summation can be simplified so that the above integral can be expressed in terms of four different integrals. The total energy per unit volume can then

be written as

$$\frac{F_{\rm lattice}}{V} = \frac{Bd^2}{(K-1)\,(N-1)\;4\pi^2\,L_bL_d}\Bigg[2\sum_{k>l}^{K}\sum_{l=1}^{K}\sum_{n>m}^{N}\sum_{m=1}^{N}\int_{-\infty}^{\infty}\mathrm{d}p_1\mathrm{d}p_2\,\mathcal{U}(p_1,p_2)e^{ip_1(k-l)L_b}e^{ip_2(n-m)L_d}$$
$$+N\sum_{k>l}^{K}\sum_{l=1}^{K}\int_{-\infty}^{\infty}\mathrm{d}p_1\mathrm{d}p_2\,\mathcal{U}(p_1,p_2)e^{ip_1(k-l)L_b}$$
$$+K\sum_{n>m}^{N}\sum_{m=1}^{N}\int_{-\infty}^{\infty}\mathrm{d}p_1\mathrm{d}p_2\,\mathcal{U}(p_1,p_2)e^{ip_2(n-m)L_d}$$
$$+NK\int_{-\infty}^{\infty}\mathrm{d}p_1\mathrm{d}p_2\,\mathcal{U}(p_1,p_2)\Bigg] \tag{4.38}$$

The first integral relates to the interaction energies of dislocation lines which have components of separation along both the x_1- and y_1- directions. The second integral relates to the interaction energies of the dislocation lines in an array along the x_1- direction. There are N such arrays. The third integral relates to the interaction energies of the dislocation lines in an array along the y_1- direction. There are K such arrays. The last integral in the above equation relates to the elastic energies of the individual dislocation lines. There are NK dislocation lines in the lattice.

4.3.2 The lower critical field h_{c1}

The lower critical field h_{c1} is defined as that value of the chiral field h, where it becomes energetically favourable to create a single dislocation in the uniform smectic phase. At the transition from the smectic phase to the TGB phase, the dislocation density is low, and therefore the distances between the individual dislocation lines (l_b and l_d) are large. Then we can ignore the dislocation interaction terms in the free energy Eq. (4.38). Then, the Gibbs free energy of the system may be written as [1]

$$\frac{G_{\rm tgb}}{V} = \frac{1}{l_b\,l_d}\left(f_{el}^{(1)} - h\,d\right), \tag{4.39}$$

where $f_{el}^{(1)} = F_{el}^{(1)}/L$ is the elastic free energy per unit length of a single dislocation line (see Eq. (4.23)). The smectic phase becomes unstable to the TGB phase when $G_{\rm tgb}/V$ becomes zero. This gives us an expression for the lower critical field h_{c1}:

$$h_{c1} = \frac{f_{el}^{(1)}}{d} \tag{4.40}$$

Since the minimum energy dislocation line in the SmC phase is a mixed dislocation line, in the above expression, $f_{el}^{(1)}$ is the elastic free energy per unit length of a mixed dislocation line, unlike the equivalent expression for SmA (see [1]).

4.3.3 The structure of the TGB$_C$ phase

We evaluate $G_{\rm tgb}/V$ (including the interaction terms in Eq. (4.38)) for a *rectangular reference lattice*. A plot of $G_{\rm tgb}/V$ as a function of l_b is shown in Fig. 4.9. We find that for large enough lattice sizes, *a lattice made up of screw dislocations has the lowest energy*. The lowest energy rectangular lattice is not a square lattice ($l_b = l_d$). This is in contrast with the result obtained for TGB$_A$. The method developed in Section 4.3.1 is general, and easily extended to arbitrary oblique lattices. Detailed numerical exploration of the energetics of arbitrary oblique lattices is in progress.

Figure 4.10 shows plots of l_b and l_d which minimize the Gibbs free energy for a TGB$_C$ structure corresponding to a rectangular reference lattice made of screw dislocations. Here, E is the elastic energy for a single screw dislocation. We can clearly see that in the TGB$_C$ phase, $l_b \neq l_d$. This is expected, since the interaction potential between dislocation lines in SmC (see Fig. 4.6) is anisotropic.

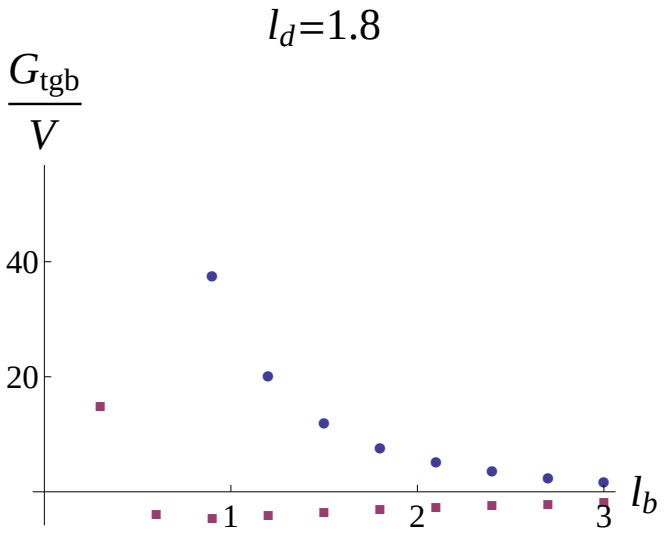

Figure 4.9: The Gibbs free energy per unit volume G_{tgb}/V (measured in units of $Bd^2/4\pi^2\,\tilde{\lambda}_c^2$) for a 100×100 lattice of dislocation lines, as a function of l_b, for $l_d = 1.8$. Distances are measured in units of $\tilde{\lambda}_c$. G_{tgb}/V for the lattice made of screw dislocation lines ($\gamma = 0$) is shown in purple, and that for the lattice made of the minimum energy dislocation lines ($\gamma = 6\pi/25$) is shown in blue. The plots are for $\delta = -0.75$, $h\,d = 15$, $\xi^{-1}\tilde{\lambda}_c = 1$ and $\beta = 3$.

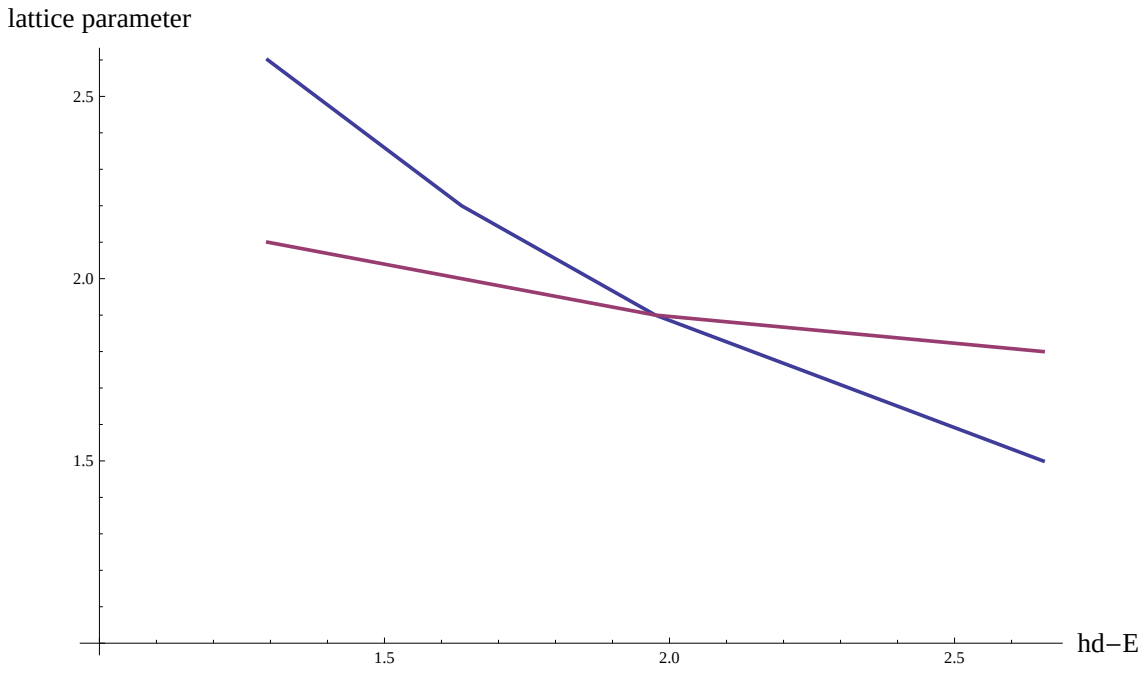

Figure 4.10: The lattice parameters l_b (blue) and l_d (purple) (measured in units of $\tilde{\lambda}_c$) as a function of $(h\,d - E)$ (measured in units of $Bd^2/4\pi^2$) close to the lower critical field, obtained by numerically minimizing Eq. (4.35) for a TGB$_C$ structure made of screw dislocations. Here, $\delta = -0.75$, $\beta = 3$ and $\xi^{-1}\tilde{\lambda}_c = 1$.

Bibliography

[1] P. M. Chaikin and T. C. Lubensky. *Principles of Condensed Matter Physics*. Cambridge University Press, Cambridge, England, 1995.

[2] A. Kundagrami. *The structure of the* $\mathrm{TGB_C}$ *phases near the upper critical twist* k_{c2}. PhD thesis, AA(University of Pennsylvania), 2003.

[3] John Price Hirth and Jens Lothe. *Theory of Dislocations*. Krieger Publishing Company, second edition, 1992.

[4] I. Bluestein, R. D. Kamien, and T. C. Lubensky. *Phys. Rev. E*, 63:061702, 2001.

[5] A. Kundagrami and T. C. Lubensky. *Phys. Rev. E*, 68:060703, 2003.

[6] L. Navailles, R. Pindak, P. Barois, and H. T. Nguyen. *Phys. Rev. Lett.*, 74:5224, 1995.

[7] Y. Hatwalne P. A. Pramod and N. V. Madhusudana. *Phys. Rev. E.*, 56:R4935, 1997.

[8] P. A. Pramod. *New Defect Structures in Liquid Crystals*. PhD thesis, Raman Research Institute, 1998.

[9] F. C. Frank. *Disc. Faraday Soc.*, 25:19, 1958.

[10] P. G. de Gennes and J. Prost. *The Physics of Liquid Crystals*. Oxford University Press, New York, USA, 1997.

[11] L. D. Landau and E. M. Lifshitz. *Statistical Physics, Part I*, volume 5 of *Course of Theoretical Physics*. Butterworth, Cambridge, England, third edition, 1980.

[12] A. Saupe. *Mol. Cryst. Liq. Cryst.*, 7:59, 1969.

[13] Orsay Group on Liquid Crystals. *Solid State Commun.*, 9:653, 1971.

[14] de Gennes P. G. *Solid State Commun.*, 10:753, 1972.

[15] A. Caille. *C. R. Acad. Sci. Ser. B*, 274:891, 1972.

[16] James F. Annett. *Superconductivity, Superfluids, and Condensates*. Oxford Master Series in Condensed Matter Physics. Oxford University Press, USA, first edition, 2004.

[17] S. R. Renn and T.C. Lubensky. *Phys Rev. A.*, 38:2132, 1988.

[18] Y. Hatwalne and T. C. Lubensky. *Phys. Rev. E*, 52:6240, 1995.

[19] P. G. de Gennes. *Mol. Cryst. Liq. Cryst.*, 21:49, 1973.

[20] F. Jahnig and F. Brochard. *J. Phys. (Paris)*, 35:301, 1974.

[21] J. Chen and T. C. Lubensky. *Phys. Rev. A*, 14:1202, 1976.

[22] G. Grinstein and R. A. Pelcovits. *Phys. Rev. Lett.*, 47:856, 1981.

[23] J. W. Goodby, M. A. Waugh, S. M Stein, E. Chin, R. Pindak, and J. S. Patel. *Nature (London)*, 337:449, 1989.

[24] K. J. Ihn, J. A. N. Zasadzinski, R. Pindak, A. J Stanley, and J. Goodby. *Science*, 258:275, 1992.

[25] I. Dozov. *Phys. Rev. Lett.*, 74:4245, 1995.

[26] R. D. Kamien and T. C. Lubensky. *J. Phys. I (France)*, 3:2131, 1993.

[27] L. Navailles, B. Pansu, L. Gorre-Talini, and H. T. Nguyen3. *Phys. Rev. Lett.*, 81:4168, 1998.

[28] T. C. Lubensky and S. R. Renn. *Phys. Rev. A*, 41:4392, 1990.

[29] L. Navailles and P. Barois. *Liquid Crystals*, 36:1241, 2009.

[30] H. T. Nguyen, A. Bouchta, L. Navailles, P. Barois, N. Isaert, RJ. Twieg, A. Maaroufi, and C. Destrade. *J. Phys. II France*, 2:1889, 1992.

[31] A. Bouchta, H. T. Nguyen, L. Navailles, P. Barois, C. Destrade, F. Bougrioua, and N. Isaert. *J. Mater. Chem.*, 5:2079, 1995.

[32] S. R. Renn. *Phys. Rev. A*, 45:953, 1992.

[33] A. Reibero, P. Barois, Y. Galerne, L. Oswald, and D. Guillon. *Euro. Phys. J.*, B11:121, 1999.

[34] Y. Galerne. *Euro. Phys. J.*, E3:355, 2000.

[35] R. Pratibha P. A. Pramod and N. V. Madhusudana. *Current Science*, 73:1997, 761.

[36] R. Shao, J. Pang, N. Clark, J. Rego, and D. Walba. *Ferroelectrics*, 147:255, 1993.

[37] J. Fernsler and OTHERS. *PNAS*, 102:14191, 2005.

[38] I. Lukyanchuk. *Phys. Rev. E*, 57:574, 1998.

[39] G. N. Watson. *A Treatise on the Theory of Bessel Functions*. Cambridge University Press, Cambridge, United Kingdom, second edition, 1944. , page 183.

[40] M. Abramowitz and I. A. Stegun. *Handbook of Mathematical Functions*. Courier Dover Publications, New York, 1965.

[41] R. Pratibha Surajit Dhara and N. V. Madhusudana. *Ferroelectrics*, 277:13, 2002.

[42] L. D. Landau and E. M. Lifshitz. *Theory of Elasticity*, volume 7 of *Course of Theoretical Physics*. Butterworth Heinemann, Oxford, England, third edition, 1986.

[43] D. Johnson and A. Saupe. *Phys. Rev. A*, 15:2079, 1977.

[44] G. Strangi, D. A. Coleman, J. E. Maclennan, M. Copic, and N.A. Clark. *Appl. Phys. Lett.*, 78:1532, 2001. and references therein.

[45] A. Tang, D. Konovalov, J. Naciri, B. R. Ratna, and S. Sprunt. *Phys. Rev. E*, 65:010703(R), 2001. and references therein.

[46] V. A. Raghunathan M. A. Kamal, A. Pal and M. Rao. *Europhys Lett.*, 95:48004, 2011.

[47] T. C. Lubensky and F. C. Mackintosh. *Phys. Rev. Lett.*, 71:1565, 1993.

[48] T. C. Lubensky T. C. Chen and F. C. Mackintosh. *Phys. Rev. E*, 51:504, 1995.

[49] Kheya Sengupta, V. A. Raghunathan, and Yashodhan Hatwalne. *Phys. Rev. Lett.*, 87:055705, 2001.